Journal of Materials Science & Nanotechnology
Volume 4 | Issue 1
ISSN: 2348-9812

Review Article Open Access

A Review on Nanoprobes for Sensing, Imaging and Disease Detection

Mazumder S[*1] and Pavurala N[2]

[1]Department of Chemical Engineering, Birla Institute of Technology and Sciences, Pilani, Rajasthan, India
[2]Department of Chemical Engineering, Virginia Polytechnic Institute and State University, Blacksburg, VA, USA

[*]**Corresponding author:** Mazumder S, Department of Chemical Engineering, Birla Institute of Technology and Science, Pilani, Rajasthan, India 333031, Fax: +91 1596-244183, Tel: +91-1596-515725 (O), +91-8239818405 (M), E-mail: sonal.mazumder@pilani.bits-pilani.ac.in

Citation: Mazumder S, Pavurala N (2016) A Review on Nanoprobes for Sensing, Imaging and Disease Detection. J Mater Sci Nanotechnol 4(1): 104. doi: 10.15744/2348-9812.4.104

Received Date: September 25, 2015 **Accepted Date:** January 27, 2016 **Published Date:** January 29, 2016

Abstract

This review focuses on imaging, visualization and detection of diseases using nanoprobes. Several currently available nanoprobes such as fluorescent nanoprobes, upconversion nanoparticle probes, supermagnetic iron oxide nanoprobes, and polymer- and liposome based nanoprobes are discussed. This paper also briefly summarizes the methodologies used to image and track single cells, tumors, cancer cells, brain diseases and angiogenic vasculature. Current challenges and future scopes of research are also discussed.

Keywords: Imaging; Tracking; Nanoprobes; Diseases; Cells; Molecules; Functionalization; Therapy; Challenges

Bioaffinity nanoprobes

A nanoprobe is an optical device that can be used to distinguish and study a chemical and/or biological sample often at the nanometer scale. Nanoprobes are usually developed by tapering an optical fiber to a tip measuring 100 nm wide. An example of the use of nanoprobes for visualization is a very thin coating of silver nanoparticles (NPs) helps to enhance the rapid oscillation of electrons during the Raman scattering effect of the light. This increases vibration energy, thereby enhancing Raman scattering. This technique is commonly known as surface-enhanced Raman scattering (SERS). The nanoprobes result in accurate detection and analysis of a sample by producing higher electromagnetic fields and higher signal output. Some of the other examples of nanoprobes are nanoparticles in aqueous solution in electrospray ionization mass spectrometry [1], extracting nanoquantities of neurochemicals via *in vivo* microdialysis [2], and using gold-based metallic nanoprobes for Theranostics [3]. Recently there has been considerable interest for ultrasensitive biodetection via optical, electrochemical, and various other means [4]. Such bioaffinity nanoprobes are particularly interesting due to comparable sizes of nanomaterials and biomolecules which can be used for highly sensitive and selective biosensing. For an example, a diagnostic method involves placing a patient's blood sample on a small chip that contains the special nanoprobes. The nanoprobes then attach to any disease markers in the blood sample, such as a cancer cell. When a laser is shined on the chip, the attached probes emit light, which is detected by an optical sensor [5]. There have been numerous nanoprobes developed for ultrasensitive bioaffinity sensing of proteins and nucleic acids during last one decade. Here we review several nanoprobes that are currently available in disease detection including fluorescent nanoprobes (organic dyes, fluorescent proteins, quantum dots (QDs) and gold nanoprobes), upconversion nanoparticle probes, superparamagnet iron oxide nanoprobes, single walled nanotubes, polymer-based nanoprobes, More specifically, we categorize them according to the major types of diseases and discuss clinical potentials and pitfalls.

Nanoprobes avilable for disease detection

Fluorescent nanoprobes

Fluorescent nanoprobes are used to detect particular components of complex biomolecular assemblies, such as live cells, with exquisite sensitivity and selectivity [6]. Fluorescence occurs in three stages within certain molecules (generally polyaromatic hydrocarbons or heterocycles) called fluorophores. A fluorescent probe is designed to respond to a specific stimulus or to localize within a specific region of a biological specimen. The process responsible for the fluorescence of fluorescent probes is illustrated by the simple electronic-state diagram (Jablonski diagram) shown in Figure 1.

The fluorophore structure and its chemical environment affects the absorbed wavelengths, energy transfer efficiency, and time before emission as the molecule in its excited state interacts with surrounding molecules.

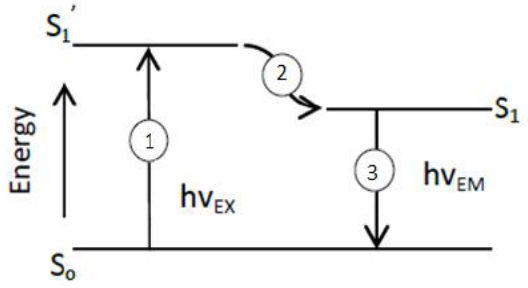

Figure 1: Jablonski diagram showing transition of energy for fluorescence [6]

Since tissues do not have a strong fluorescence contrast, exogenous fluorescent probes have to be administered *in vivo* to visualize living tissues in its native physiological state. For efficient imaging, the probes must be stable in the *in vivo* environment, and accumulate and produce imaging contrast at the target site. Fluorescent probes are divided into non-specific, targeting and activatable probes (Figure 2) according to the mechanism of contrast generation [7].

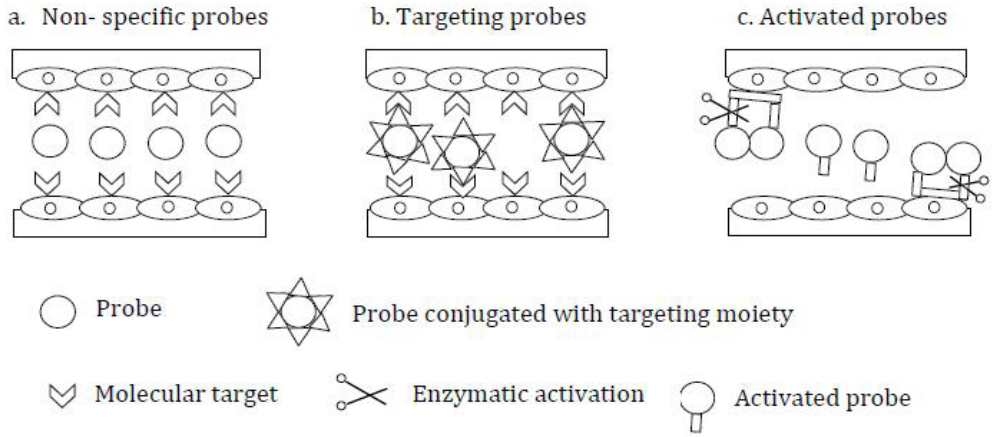

Figure 2: Schematic representation of types of fluorescent probes according to contrast generation; **a)** Non-specific compartmental distribution of the probes; **b)** Targeted binding of probes via surface ligands to molecular targets; **c)** Activatable probes quenched in their native state and become fluorescent by enzyme-mediated cleavage [7]

Different kinds of fluorescent probes are explored for disease detection. The major types such as organic dyes, fluorescent proteins, quantum dots and gold nanoprobes are discussed in the following section.

Organic dyes: Organic dyes or conventional near infrared (NIR) dyes that fluoresce in the near infrared region have attracted much attention in last several years. However, they have several limitations such as poor hydrophilicity, low photostability, small quantum yield (QY) and instability in the bio-environment [8-11]. Recently such organic dyes are encapsulated in various nanoparticles to overcome these intrinsic limitations. Some of the recent and interesting works are described here.

In 2008, Wu *et al.* developed conjugated polymer dots (Pdots) which are small nanoparticles with extraordinary fluorescence brightness and excellent photostability [12]. The sizes of Pdots are as low as 4 nm and they can be encapsulated and functionalized. Pdots are interesting because they have the highest fluorescence brightness/volume ratios due to their high absorption cross sections, high radiative rates, high effective chromophore density, and minimal levels of aggregation-induced fluorescence quenching.

Organic dyes themselves can also be directly assembled into pure dye NPs. Recently, small-molecule organic dye nanoparticles (ONPs) have been developed as a new class of promising fluorescent probes [12-15]. These ONPs can be used to encapsulate NIR dyes to enable efficient fluorescence resonance energy transfer (FRET) to obtain NIR probes with remarkably enhanced performance for *in vitro* and *in vivo* imaging. In comparison with pure NIR dyes, ONPs mediate almost 50-fold increased brightness, large Stokes shifts (w250 nm) and dramatically enhanced photostability. Further, the NIR-emissive ONPs can have water-dispersity and size- and fluorescence- stability over pH values from 2 to 10 for almost 60 days on surface modification. They can also be used for highly efficient folic-acid aided specific targeting *in vivo* and *ex vivo* cellular imaging [16]. These nanoparticles shows negligible toxicity during *in vivo* imaging [17]. An example can be a class of water-miscible ONPs consisting of 1, 4-dimethoxy-2, 5-di [40-(cyano)styryl]benzene (COPV, Figure 3). These could overcome the limitations of two-photon absorption (TPA) organic dyes such as water insolubility and strong fluorescence quenching in aqueous media due to the self-aggregation effect [16,18]. COPV J-aggregate ONPs are 3–4 orders of magnitude brighter than conventional fluorescent dyes and an order of magnitude brighter than QDs. Moreover, these ONPs exhibit no obvious cytotoxicity at concentrations as high as 100 μg/ml [19]. Thus, ONPs are a highly selective probe for diagnostic purposes.

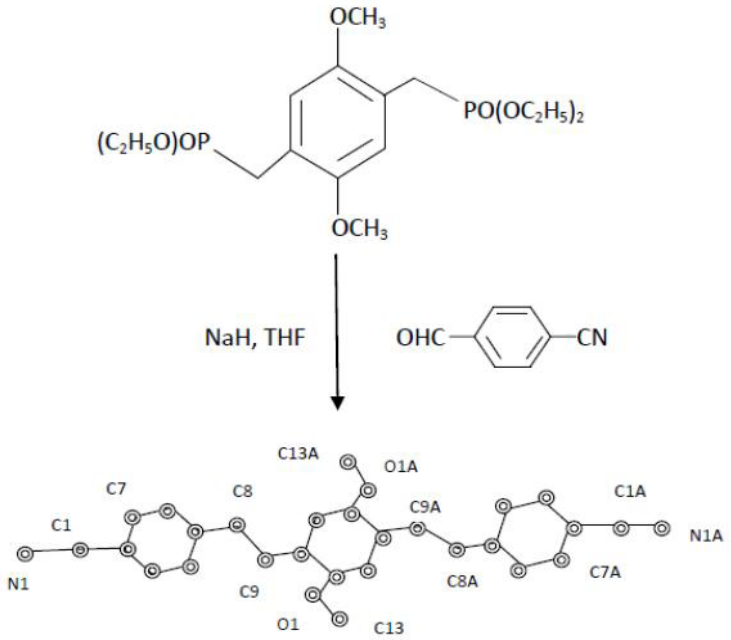

Figure 3: A single crystal structure of COPV synthesized with one end functionalized with cyano groups [18]

Indocyanine green (ICG) is a tricarbocyanine dye that exhibits absorption and emission maxima around 740 and 800 nm [20,21]. It is the only NIR organic dye clinically approved by the U.S. Food and Drug Administration (FDA) for human medical imaging and diagnosis [22] and as a fluorescence probe and photosensitizing agent [23]. Despite clinical approval, ICG has low absorptivity by tissue chromophores, poor aqueous stability *in vitro*, concentration-dependent aggregation, rapid elimination from the body, and lack of target specificity [24]. To overcome these limitations, folate receptor targeted, ICG dye-doped poly (D,L-lactide-co-glycolide) (PLGA) lipid NPs (FA-ICG-PLGA-lipid NPs) were constructed using a single-step self-assemble and nanoprecipitation method. The prepared FAICG-PLGA-lipid NPs exhibit good biocompatibility, and monodispersity, excellent NIR penetration ability, significant stability against photobleaching and long circulation time [25]. A more stable alternative to ICG with higher fluorescence intensity is IR-780 dye which is a lipophilic cation heptamethine dye [26]. IR-780 can be utilized in photothermal therapy with laser irradiation. It is an important theranostic agent, but its lipophilicity limits its application. To address this problem, multifunctional heparine folic acid-IR-780 nanoparticles (HF-IR-780 NPs) were synthesized by self-assembly of the heparine folic acid conjugate and IR-780 using the ultrasonic sound method [27]. The HF-IR-780 NPs could be used simultaneously for NIR fluorescence imaging and photothermal therapy *in vitro* and *in vivo* for folate-overexpressed tumors [27].

Fluorescent proteins: Fluorescent proteins (FPs) are a structurally homologous class of proteins that can form visible wavelength chromophores from a sequence of three amino acids within their own polypeptide sequence. Biologists often introduce a gene encoding an engineered fluorescent protein into living cells and subsequently visualize the location and dynamics of the gene product using fluorescence microscopy.

NIR FPs with a silica nanoshell (NIRFP@silica) have been shown to have a QY of 0.33 when used for *in vivo* imaging. The silica shell not only protects NIR FPs from denaturation and metabolic digestion, but it also enhances the QY and photostability of the coated NIR FPs. In a mouse model, NIRFP@silica NPs, injected *via* the tail vein were distributed throughout the mouse body, and were efficiently eliminated through urine within 24 h. This experiment demonstrated safety and robustness of this NIR fluorescence probe for whole body imaging [28].

In another study, a tetrameric far-red fluorescent protein (tfRFP) was used as a scaffold to create a self-assembled octavalent peptide fluorescent nanoprobe (Octa-FNP). *In vitro* studies showed that Octa-FNP is a 10-nm fluorescent probe with excellent serum stability. Cellular uptake of Octa-FNP by human nasopharyngeal cancer was 15-fold greater than that of a tetravalent probe, ~80-fold greater than that of a monovalent probe and ~600-fold greater than that of a nulvalent tfRFP. *In vivo* enhanced tumor targeting and intracellular uptake of Octa-FNP have been confirmed using optical imaging and Western blot analysis. A high contrast of Octa-FNP signal between tumor tissue and normal organs was achieved and Octa-FNP was seldom detected in liver and spleen. The easy preparation, precise structural and functional control, and multivalent effect of Octa-FNP make it a powerful tool for tumor optical molecular imaging and for evaluating the targeting ability of numerous peptides *in vivo* [29]. Green fluorescent proteins (GFP) are used as fluorescent probes for temperature probing (Figure 4).

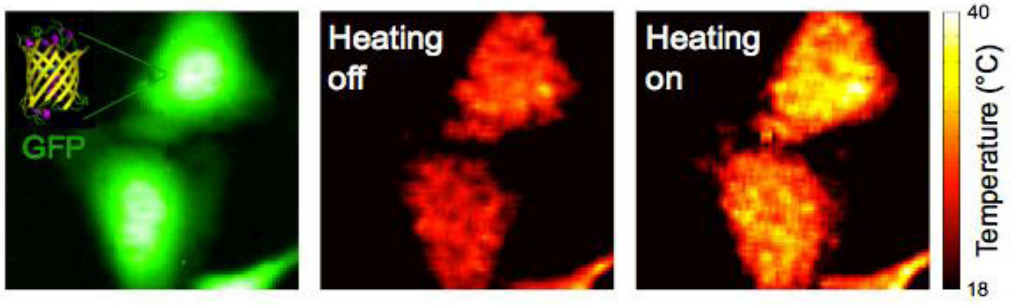

Figure 4: Green fluorescent proteins (GFPs) as a thermal nanoprobes suited for intracellular temperature mapping. Temperature probing is achieved by monitoring the fluorescence polarization anisotropy of GFP [30]

Fluorescent dendritic nanoprobes: Several studies have reported the use of dendrimers as scaffolds for fluorophores and functional groups for bioconjugation [31-34]. Some notable examples are polyphenylene dendrimers [31,32], and polyaminoamine (PAMAM) dendrimers [33]. In addition, Kim *et al.* [35] describes the synthesis, photophysical characterization, and application of a new class of fluorescent probes called fluorescent dendritic nanoprobes (FDNs). FDNs have properties similar to those of fluorescent proteins, and they are larger than single fluorescent dyes but smaller than QDs. FDNs have better water-solubility, brightness, and bioconjugation than conventional dendrimer fluorophores. They are also easy to prepare. FDNs consist of generation-5 and generation-6 PAMAM dendrimers. An example of biodegradable pH sensitive dendritic probe is shown in Figure 5. FDNs offer the combined advantages of enhanced photophysical properties and small nanoscale dimensions, which can benefit a wide array of advanced high-resolution imaging techniques and subdiffraction localization methods [35]. Therefore they hold strong potential to serve as a new class of fluorescent probes for biological assays and imaging.

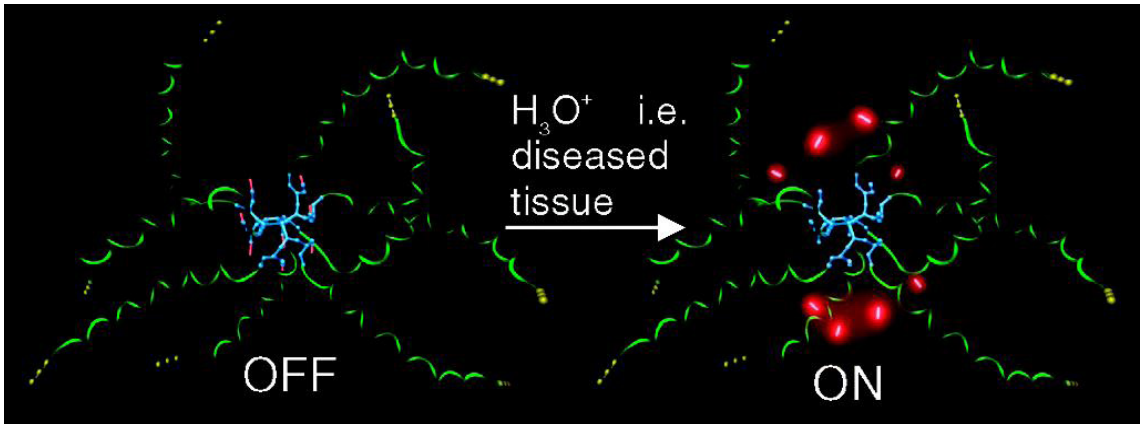

Figure 5: Biodegradable pH sensing dendritic nanoprobe OFF: neutral pH, healthy tissue, ON: acidic pH, diseased tissue [36]

Quantum dots (Qds): QDs are nanocrystals composed of semi-conducting materials [37]. Typically, QDs are ~2–20 nm in diameter depending on the core composition and the surface coating or functionalization. Most of the QDs reported to date have a core/shell structure with the core composed of atoms from periodic groups II–VI (CdSe, CdTe, CdS, PbSe, ZnS and ZnSe), III–V (GaAs, GaN, InP, InAs), and IV–VI (PbS). For biological applications, QDs have many properties that are superior to those of organic fluorophores and fluorescent proteins, including strong resistance to photobleaching, continuous absorption spectra covering the UV to NIR region, narrow emission spectra, large effective Stokes shifts, long fluorescence lifetimes, and excellent multiphoton emission [38,39]. They are chemically grown and their emission properties which are related to the confinement effect of an electron-hole pair (exciton) within the crystal mainly depend on their shape and size [40]. The fluorescent emission wavelengths of QDs ideally should be around 700–1000 nm for *in vivo* imaging in the NIR region to minimize endogenous fluorescence and interference from major absorbers in the body (nanomaterials).

Li *et al.* first used silicon based QDs (Si QDs) for biological applications to label Chinese hamster ovary cells for *in vitro* imaging [41]. In another study, these Si QDs were loaded with the anti-cancer drug doxorubicin (D-LPSiNPs) and delivered into BALB/c mice and the accumulation and degradation *in vivo* was monitored (Figure 6) [42].

In another work by Nurunnabi *et al.* [43] the surfaces of NIR QDs have been modified to achieve water solubility and target specific properties. This was done by the solid dispersion method using polyethylene gycol - 10, 12-pentacosadiynoic acid (PEG – PCDA) and PCDA - herceptin conjugates. The micelles which were formed were spherical with diameters of around 130 - 150 nm. The neighboring PCDA-herceptin moieties crosslinked upon UV irradiation leading to stabilization of the QD cores located within the nanoprobes [43]. They could be used for both active and passive targeting and imaging and treatment of cancer.

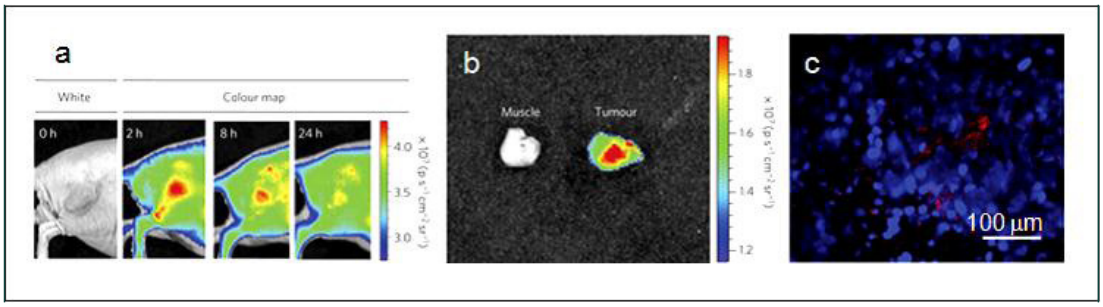

Figure 6: **a)** Representative fluorescence images of a mouse with an MDA-MB-435 tumor; The mouse was imaged using a 615–665 nm excitation filter and an 810–875 nm emission filter at the indicated time post-intravenous injection of D-LPSiNPs (20 mg/kg). A strong signal from D-LPSiNPs was observed in the tumor, indicating significant passive accumulation in the tumor by the enhanced permeability and retention (EPR) effect; **b)** *Ex vivo* fluorescence images of the tumor from the mouse used in (a); **c)** Fluorescence images of a tumor slice from the mouse in (a). Red and blue indicate D-LPSiNPs and cell nuclei (DAPI stain) [42].

Gold nanoprobes: In the past decade, the florescent properties of gold and silver nanoclusters (NCs) have shown potential as efficient optical probes [46-52]. They have high chemical stability and biocompatibility and are used for sensing [53-55], biolabeling [56,57] and bioimaging [58].

Gold nanoclusters (AuNCs) are synthesized by chemical reduction of Au precursors in the presence of thiol stabilizers to generate AuNCs that fluoresce in the blue to NIR regions [59-63]. These NCs exhibit low QY (0.001–0.1%).

NIR AuNCs are produced by stabilizing the core of 6-nm diameter gold nanoparticles with dihydrogenlipoic acid (DHLA) (AuNC@DHLA) [64,65]. Conjugation of AuNC@DHLA with biomolecules is achieved using the carboxyl group on DHLA via carbodiimide chemistry. Polyethylene glycol (PEG, 5 kDa), PEG-biotin and avidin have been attached in this manner. Although the QY of these NCs is low ~1–3%, they can be used to specifically label human hepatoma cells (HepG2) and to monitor the non-specific uptake of AuNCs by human aortic endothelial cells. The results indicate that these AuNCs are relatively nontoxic.

Biocompatible AuNCs are prepared via aqueous synthetic routes with biological molecules [66]. For example, bovine serum albumin (BSA) is used to prepare AuNCs (consisting of 25 gold atoms with red emission [67] (Figure 7a). The QY of the NIR AuNCs produced by this method is low (0.1%). Despite this, *In vivo* tumor fluorescence imaging is done using MSD-MB-45 and HeLa tumor xenograft models show high accumulation in the tumor areas due to EPR effects (Figure 7b) [68].

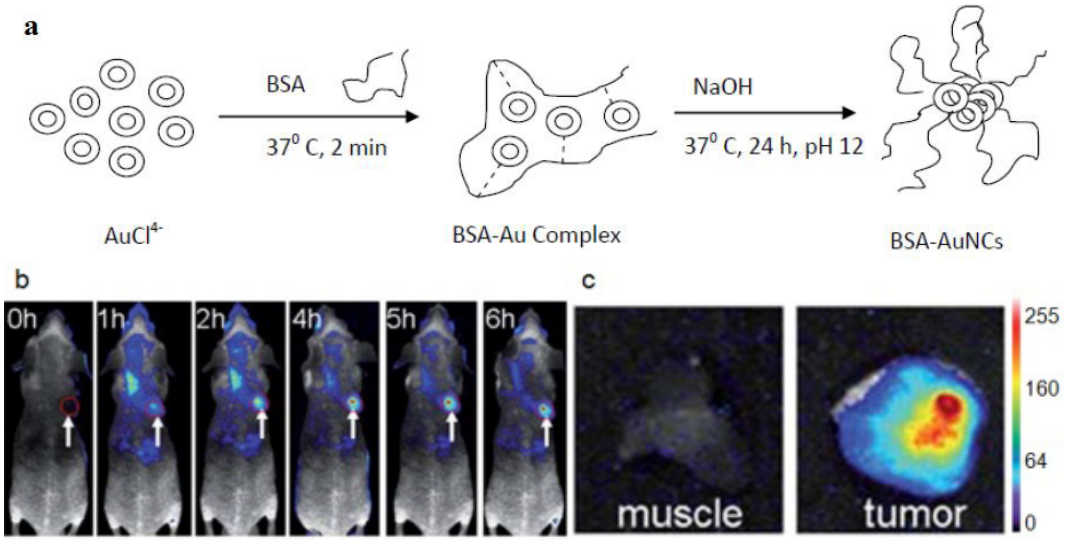

Figure 7: **a)** Schematic of the synthesis of AuNCs in BSA solution [67]; **b)** Fluorescence images of mice with a MDS-MB-45 tumor. A strong signal from AuNCs in the tumor indicated by a red circle in the figure showing significant passive accumulation in the tumor via the EPR effect. White arrows indicate the tumor site; **c)** *Ex vivo* fluorescence image of the muscle and tumor tissue around the tumor from the mice used in (b) [68].

Gold nanoparticles have been specifically used to detect oligonucleotide sequences after being bound to nucleic acids through a thiol linkage [69]. The basis of the detection process of functionalized gold nanoprobes is to hybridize them specifically to their complementary target sequences, which causes a change in the surface plasmon resonance (SPR).

A new class of multifunctional gold nanoprobes for ultra-sensitive optical detection of reactive oxygen species (ROS) and hyaluronidase (HAdase) [70] was described recently. The nanoprobes are fabricated by immobilizing nNIRF dye labeled hyaluronic acid (HA) onto the surface of goldnanoparticles (AuNPs). The nanoprobes effectively induced NP surface energy transfer (NSET) between NIRF dyes and AuNPs. When the surface immobilized HA is cleaved by ROS and HAdase, strong fluorescence recovery signals are obtained with extreme sensitivity. In live animal models of rheumatoid arthritis (RA) and metastatic tumors, local arthritic inflammation and tumor sites were clearly identified upon systemic injection of the nanoprobes. These results suggest that these gold nanoprobes can be exploited not only as *in vitro* molecular and cellular imaging sensors for ROS and HAdase, but also as *in vivo* optical imaging agents for detection of local HA degrading diseases such as RA and tumors.

AuNP entrapped in a folic acid-modified dendrimer (Au DENPs-FA) - have been used as nanoprobes for *in vitro* and *in vivo* targeted computed tomography (CT) imaging [71]. The micro CT images revealed that the SPC-A1 cells were detected under X-ray after incubation with the Au DENPs-FA *in vitro.* Imaging of xenograft tumor model was possible administration of the particles via intravenous, intratumoral, and intraperitoneal route. Transmission electron microscopy data suggested that the lysosomes of the cells could dominantly uptake the AuDENPs-FA.

The low quantum yield of gold nanoparticles is mainly attributed to the size and capping agent of the nanoparticles. In polymer-stabilized gold clusters of 2.2–3.4 nm diameter the polymer to gold ratios were varied in order to tune the properties of fluorescence emission. There a quantum yield of 3% was achieved [72]. The highest quantum yield of ~ 41% has been reported for Au8 nanoprobes stabilized in dendrimer aqueous solution [73]. It is observed that the photoluminescence efficiency tends to decrease when the size of nanoprobes increases, and it is argued that clustering, surface modification of nanoprobes, and imbedding/stabilizing by the medium can influence the observed fluorescence signals [72-74]. The results so far obtained are mainly for clustors of diameter around 100 nm and not of individual particles.

Upconversion nanoparticle probes

Upconversion nanoparticles (UCNPs) are new generation fluorophores that have the ability to convert NIR radiations with lower energy into visible radiations with higher energy via a nonlinear optical process. Recently, these UNCPs have been used as alternatives to traditional fluorophores, as they show great potential for imaging and biodetection assays in both *in vitro* and *in vivo* applications. Their unique luminescent properties, including high penetration depth into tissues, low background signals, large Stokes shifts, sharp emission bands, and high resistance to photobleaching overcome the current limitations of traditional fluorescent probes [75]. UCNPs, particularly lanthanide-doped rare-earth nanocrystals, also have great potential in biomedical imaging due to their sharp emission bandwidth, long lifetime, tunable emission, high photostability, and low cytotoxicity [76-78]. More importantly, UCNPs NIR utilize excitation within the "optical transmission window" of biological tissues (700 - 1000 nm); there by significantly enhancing penetration depths and minimizing background autofluorescence, photobleaching and photodamage to biological specimens [79-83].

Neurotoxin-mediated UCNPs have been developed for tumor targeting and visualization in living animals [84]. Laser scanning upconversion fluorescence microscopy was used to visualize nanoprobes that specifically targets glioma cells. The intravenous injection of the nanoprobes in a balb c mice resulted in high-contrast images demonstrating highly specific tumor binding and direct tumor visualization with bright red fluorescence under 980-nm NIR irradiation. The high sensitivity and high specificity of the neurotoxin-mediated upconversion nanoprobes and the simplification of the required optical device for tumor visualization suggest an approach that may help improve the effectiveness of the diagnostic and therapeutic modalities available for tumor patients.

Multifunctional UCNPs made of Er/Yb-doped NaYF4 core and NaGdF4 shell was used to target cancer cell nuclei as well as deliver the anticancer drug directly to the nuclear region [85]. The real-time imaging of the cell nuclei was done by magnetic resonance (MR)/upconversion fluorescence. These particles showed enhanced upconversion fluorescent imaging and more sensitive T_1-MR imaging performances. They were used to improve the efficacy of DOX in Hela tumor models, by directing DOX delivery to the nucleus under the synchronous monitoring of the nanoparticles.

Zeng *et al*. constructed multi-functional nanoprobe consisting of PEG modified BaGdF5:Yb/Er UCNPs [86]. These nanoprobes were synthesized by using facile one-pot hydrothermal method and used for bioimaging using fluorescence, CT, and MRI. Apart from superior fluorescent properties, they showed excellent paramagnetic property. These UCNPs were used as a contrast agent for improving the detection of splenic diseases, showed low cytotoxicity and long circulation time.

Liu *et al*. prepared polyacrylic acid (PAA) modified BaYbF5:Tm NPs via a solvothermal route [87]. They proved to be excellent multi modal contrast agents used for direct visualization of the GI tract with low systemic toxicity.

A covalently grafted core-shell structured UCNPs were prepared along with nanographene oxide (NGO) via bifunctional PEG and phthalocyanine (ZnPc) was loaded on the surface of NGO [88]. These UCNPs-NGO/ZnPc nanocomposites could image cells and whole-body animals with high contrast for diagnosis. They can also be used to generate cytotoxic singlet oxygen under light excitation for photodynamic therapy (PDT) and to rapidly and efficiently convert 808 nm laser energy into thermal energy for photothermal therapy (PTT). They have been shown to have high therapeutic efficiency for cancer treatment.

Superparamagnet iron oxide nanoprobe

Superparamagnetic iron oxide (SPIO) nanoprobes have proven to be a useful tool for enhancing magnetic resonance contrast to monitor anatomical, physiological and molecular changes. These probes can be used to detect inflammatory diseases via the accumulation of non-targeted SPIO nanoprobes in infiltrating macrophages and for the specific identification of cell surface markers expressed on tumors [89]. SPIO nanoprobes typically consist of two components, an iron oxide core composed of magnetite (Fe_3O_4) and/or maghemite and a hydrophilic coating. Maghemite is the ferrimagnetic cubic form of Fe (III) oxide and it differs from the inverse spinel structure of magnetite through vacancies on the cation sublattice [90]. The two iron oxide structures possess similar magnetic properties, although maghemite has a slightly lower saturation magnetization [91,92]. The sizes of these nanoprobe ranges greatly from 2 to 3 nm for citrate inhibited growth SPIO nanoprobes [93] to tens of nanometers for polymer coated polycrystalline iron oxide nanoprobes to micrometers for orally ingestible contrast agents. Larger diameters are available and are useful in such enterprises as cell tracking [94,95] and separation [96], cell rheology, and membrane deformation [97,98] and as contrast agents for the gastrointestinal tract [99], but they have limited functionality in molecular imaging applications due to their limited accessibility to the neo- and microvasculature.

A magnetic resonance imaging (MRI) scanner is responsible for altering the alignment of magnetization of particles in the body. The MRI contrast agents are divided into two parts, including T1 and T2 agents. T1 agents can alter the longitudinal (T1) relaxation times of water protons to produce bright positive signal intensity in images and increase the conspicuousness of cells. T2 agent is to alter the transverse (T2) relaxation times of water protons. T2 agents provide dark negative signal intensity in images and can be used to visualize stem cells grafted in organs that appear as high signal intensity (e.g. kidney or lymphoid tissues). Compared to T1 agents, SPIONs based T2 agents appear to be the preferred MRI contrast agents for monitoring stem cells due to their high sensitivity and excellent biocompatibility. Figure 8 describes how relaxation time changes when cells are tagged with magnetic nanoprobes.

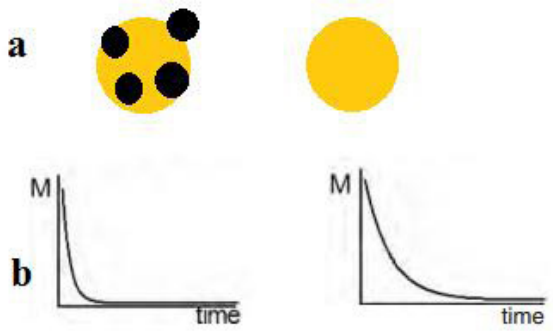

Figure 8: A qualitative graph of the changed relaxation time; **a)** Cells tagged with magnetic nanoparticles and a short relaxation time; **b)** Cells without any enhancement and thus the original relaxation time [100]

In 2011, Liu *et al*. developed SPIO nanoprobe for labeling and tracking of mesenchymal stem cells (MSCs) [101]. Low molecular weight amphiphilic polyethyleneamine of 2000 molecular weight (PEI 2k) was used to form stable nanocomplexes with SPIO nanoparticles. The probe could hold multiple SPIO nanoparticles with a controlled clustering structure, leading to much higher T2 relaxivities compared to single SPIO nanoprobes. Labeled MSCs were seen to maintain their viability, proliferation, or differentiation capacity. The iron uptake process in MSCs displayed a time- and dose-dependent behavior. Transmission electron microscopy revealed that the nanoprobes were internalized into the cytoplasm of the MSCs. When the MSCs were labeled and injected, they showed strong image contrast compared to unlabeled cells even after 2 weeks post transplantation.

SPIO nanoprobes coated with dextran and functionalized with negatively charged functionalities have been used to connect specific peptide labels by electrostatic interactions [102,103]. Furthermore, SPIO nanoprobes were shown to be incorporated by several phagocytic cells, in particular macrophages in liver and spleen, even when they had a regular dextran coat [104]. Thus SPIO nanoprobes are a promising group of imaging probes because the MR signal intensity can be manipulated and they have a favorable toxicity, and genuine potential for cellular uptake.

Single walled Nanotubes

Research showed the potential of high resolution single-walled carbon nanotube (SWNT) tips to image nanostructures with high resolution [105]. SWNT tips provide a significant improvement in lateral resolution with respect to multi-walled nanotube tips and microfabricated Si tips. Nanotube tips also can be used to resolve substructure within SWNTs deposited on surfaces. SWNT tips exhibit superior resolution compared to conventional tips when imaging biological nanostructures, such as double-stranded DNA [105].

Welsher *et al*. functionalized SWNTs with PEG and conjugated to antibodies such as Rituxan. This could selectively recognize the CD20 cell surface receptor on B-cells with little nonspecific binding to negative T-cells and to Herceptin to recognize HER2/neu positive breast cancer cells [106]. SWNT-antibody binding to cells can be imaged by detecting the intrinsic NIR photoluminescence of nanotubes. This approach shows ultralow NIR autofluorescence for various cells which is advantageous compared to high autofluorescence and large variations between cell lines in the visible spectrum. Surface functionalized SWNTs can be considered to be novel NIR fluorophores for sensitive and selective biological detections and for imaging *in vitro* and potentially *in vivo*.

Polymer-based nanoprobes

The optical properties and chemical stability of ICG are improved when it is encapsulated in different polymer or co-polymer matrices (typically with particle diameter of 100–500 nm) [107-110]. PEG-PLA nanospheres are carriers of dye [111]. Use of hydrophobic near infrared 1,1'-dioctadecyl-3,3,3',3'-tetramethylindotricarbocyanine iodide (NIR DiR) dye leads to a constant fluorescent signal in blood for up to 6 hours post injection compared to amphiphilic Nile Red dye, which is quickly released from the polymer matrix after injection and rapidly eliminated from the blood stream. DiR-loaded particles can be used for tumor labeling as well [112].

NIR fluorescence dyes encapsulated in poly(ethylene imine) or biodegradable aliphatic polyester dendrimers (typically 10–30 nm diameter) show enhanced stability, resistance to enzymatic oxidation, renal clearance and prolonged *in vivo* residence time [113,114]. They are also capable of transporting both hydrophilic and hydrophobic molecules [115], and they have low cytotoxicity.

A water-soluble, amphiphilic phospholipid polymer, poly[2-methacryloyloxyethyl phosphorylcholine (MPC)-*co*-*n*-butyl methacrylate (BMA)-*co*-*N*-succinimidyloxycarbonyl tetra(ethylene glycol) methacrylate] (PMBS), has been synthesized and conjugated with molecular beacons (MBs) to form nanoprobes *via* a chemical reaction between the ester group of *N*-hydroxysuccinimide and the amine group of the MBs. This enabled visualization of the distribution and dynamics of intracellular biomolecules and thereby provided an understanding of the mechanisms of intracellular bio-reactions. The carcinoma cells used to test this probe remained 100% viable after incubation with PMBS-MB probes. These probes exhibited high target specificity and resistance to nonspecific adsorption of proteins compared with unconjugated MBs. They also were able to penetrate the cytoplasm of the cells [116].

New hyperbranched polysiloxysilane (HBPS) materials containing terminal carboxylic acid and quaternary ammonium groups have been designed to generate fluorescent-dye-encapsulated nanoprobes. These polymers exhibited desirable characteristics, including amphiphilicity for nanoprobe formation, and contained various terminal groups for surface-charge control on the nanoprobes or for further bioconjugation for targeted imaging [117].

Liposome-based nanoprobes

Liposomes are physically and chemically well-characterized structures [118], and liposomes-based nanocarriers have been widely applied for improved molecular transport [119]. Some of their unique features have made them suitable for tumor-targeted imaging. They are capable of holding a large payload of contrast agent, and their protective bilayer shields enclosed molecules from interaction with the contents of the bloodstreams. Coating the surface of these nanoparticles with (PEG) -polymers can increase blood circulation time, resulting in EPR of contrast agents in tumor and the large surface area allows for an increased number of ligand binding sites [119-122].

The polystyrene (PS)-targeted liposomal nanoprobe, PGN-L-800CW, which contains NIR dye, (IRDye® 800CW) was developed to improve the ability of PS-targeted optical imaging probes for sensitive imaging of glioma [123].

In 2011, another liposome nanoprobe was generated by passive adsorption of ICG; and the cetuximab monoclonal antibody for epidermal growth factor receptor (EGFR) [124]. The ICG molecules adsorbed to the liposomes were more fluorescent than free ICG and had a larger QY. Cetuximab-adsorbed fluorescent liposomes preserved EGFR recognition, as was evident from internalization and selective binding to A431 colon carcinoma cells over expressing EGFR. The binding of cetuximab targeted fluorescent liposomes to A431 compared with IEC-6 cells (normal enterocytes expressing physiological EGFR levels) was greater by a factor of 3.5, ensuring sufficient imaging capabilities with available fluorescent equipment.

The above section has been summarized in Table 1 to understand his use of nanoprobes for use in certain applications.

Nanoprobes	Subcategory	Unique properties	Applications (in-vitro/in-vivo)
Fluorescent	Organic dyes nanoparticles	Extraordinary fluorescence, excellent photostability, high absorption and emission spectra, negligible toxicity.	In - vitro and In-vivo.
	Fluorescent proteins	High photostability and quantum yield.	In-vitro and In-vivo.
	Fluorescent dendritic nanoprobes	High water solubility, brightness and bioconjugation.	In-vitro, further research ongoing to use them in-vivo.

Nanoprobes	Subcategory	Unique properties	Applications (in-vitro/in-vivo)
		Strong resistance to photobleaching, continuous absorption spectra, excellent fluorescence and emission spectra.	In-vitro and in-vivo (excluding toxic materials such as CdS, CdSe etc).
	Gold nanoparticles	High chemical stability and biocompatibility.	In-vitro and in-vivo.
Upconversion nanoparticle		High resistance to photobleaching, high penetration depth, sharp emission bands, high photostability and low toxicity.	In-vitro and in-vivo.
Superparamagnet iron oxide nanoprobe		Enhance magnetic resonance contrast.	In-vitro , not in-vivo due to limited accessibility to neo and microvasculature.
Single walled nanotubes		Superior resolution, specific detection	In-vitro and in-vivo.
Polymer		Enhanced stability, resistance to enzymatic oxidation, prolonged in-vivo residence time, low cytotoxicity	In-vitro and in-vivo.
Liposome		Efficient contrast agent, high binding	In-vitro and in-vivo.

Table 1: A summary on various types of nanoprobes and their suitability in in-vitro and in-vivo applications

Use of nanoprobes to detect specific types of disease

Nanoprobes for disease detection in the brain

Nanoprobes have several advantages over small molecules in brain tumor imaging. For example, the circulation lifetime of nanoprobes can be tuned by tailoring their size, shape and surface functionalization. The prolonged circulation lifetime and the disrupted blood brain tumor barrier (BBTB) lead to the passive intratumoral accumulation of nanoprobes via the enhanced and permeable retention (EPR) effect [125]. The main strategies of endogenous molecules to circumvent the blood brain barrier (BBB) include the diffusion and transcytosis (Figure 9). Diffusion is a main strategy of small substances entering the brain. While hydrophilic molecules diffuse paracellularly through the tight junctions (TJs) with a low extent, lipophilic substances like steroid hormones traverse endothelial cells transcellularly by dissolving in the lipid plasma membrane. In addition to non-specific diffusion, compounds essential for brain homeostasis such as amino acids, glucose, and neuropeptides can diffuse into the brain via transporter mediated delivery However, intracerebral diffusion works only for small molecules with molecular weight less than 500 Da but not for nanoparticles. Transcytosis is the main pathway of endogenous macromolecules crossing BBB, which presents traversing the brain capillary ECs within endocytic vesicles from the luminal cell side to the abluminal side where exocytosis occurs. Due to the up-regulated permeability of BBTB, the passive intratumoral accumulation via EPR effect and the positive transcytosis are the main strategies of NPs to visualize gliomas [125].

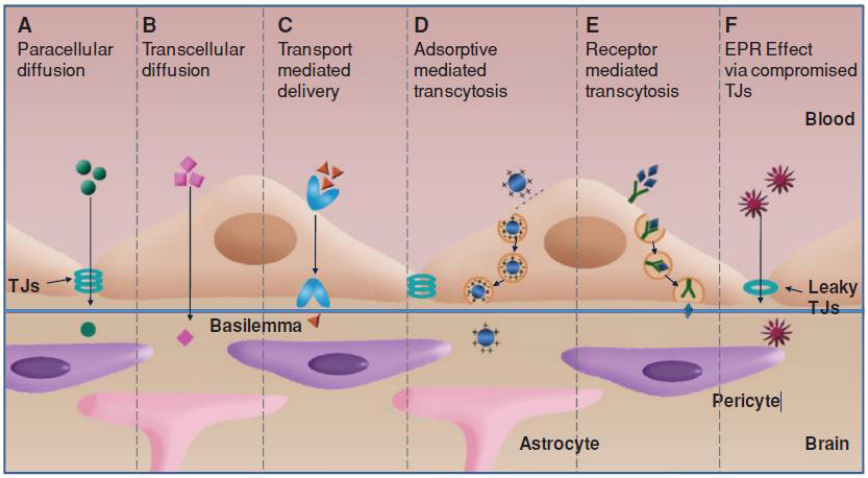

Figure 9: The BBTB crossing pathways. Small molecules usually diffuse into the brain via the pathways from "A" to "C". Nanoparticles penetrate BBTB through the trancytosis strategies such as "D" and "E". Both small molecules and the nanoparticles can traverse BBTB via EPR effect due to the compromised TJs in "F" pathway [125]

Alzheimer's disease (AD) is the most common form of brain diseases in the elderly, and it affects more than 35 million people worldwide [126,127]. Effective treatment of AD is difficult due to limitations imposed by the bloodbrain barrier (BBB) and the non-selective distribution of drugs in the brain. This also results in severe side effects. PEGylated poly (lactic acid)(PLA) polymer was used to develop a dual-functional nanoparticle drug delivery system and peptides (TGN and QSH) was conjugated to the surface of the nanoparticle [128]. These nanoparticles showed enhanced targeted delivery to the desired location in the brains of model mice infected with AD. A MTT assay confirmed low cytotoxicity of this delivery system.

Nanovehicles loaded with gadolinium (Gd) and I ((nanoparticles-IgG4.1) have been used to target cerebrovascular amyloid (CVA) [129]. These nanovehicles showed excellent distribution to the brain vasculature and target CVA. Additionally, they could carry therapeutic agents to reduce cerebrovascular inflammation associated with CVA, which is believed to trigger hemorrhage in CVA patients.

Biocompatible nanoprobes composed of a PEG-coated iron oxide NPse have been shown to be capable of specifically targeting glioma tumors via the surface-bound targeting peptide, chlorotoxin (CTX). In comparison to conventional Gd chelates, NP-based contrast agents offer prolonged delineation of tumor margins due to enhanced cellular internalization and slower clearance from the tumor site [130]. These nanoprobes with high-targeting specificity and biological response can aid in the diagnosis and treatment of gliomas and other tumors of neuroectodermal origin [130].

Metastatic disease detection

Patients suffering from ovarian cancer do not respond well to conventional therapeutics. The mortality rate of ovarian cancer remains one of the worst among all cancer types [131,132]. NIR-dye labeled magnetic nanoparticles probe was used to for imaging of HER-2 human ovarian cells by dual-modality photoacoustic and fluorescence molecular tomography (PAT/FMT) [133]. These imaging methods could help the targeted nanoprobes to map tumors in high resolution and high sensitivity.

Sentinel lymph node (SLN) imaging can be used to evaluate the metastatic status of a tumor [134-136]. In the imaging process, a contrast agent is injected near the primary tumor, and it is taken up by the adjacent lymphatic system and transported to the SLN. Vital dyes and radionuclide labeled sulfur colloids are commonly used as imaging agents [137]. Huang *et al.* recently developed mesoporous silica-based triple-modal that integrate multiple functional moieties to facilitate NIR optical, MRI and positron emission tomography (PET) imaging. The NIR dye ZW800 was used to design a nanoprobe labeled with the T_1 contrast agent Gd^{3+} and radionuclide ^{64}Cu through chelating reactions. These nanoprobes showed high stability, long intracellular retention time and therefore long-term *in vivo* imaging. This work paved the way for designing robust multifunctional nanomaterials for mapping SLNs and for tumor metastasis diagnosis [138].

Another class of nanoparticles for tumor imaging is multilayered core/shell nanoprobes (MQQ-probe) based on magnetic nanoparticles (MNPs) and QDs. These probes can be used both as a fluorescent probe and as a contrast reagent in MRI. Ma *et al.* used anti-HER2 antibody conjugated to the surface of the MQQ-probe for imaging breast cancer tumor [139]. The *in vitro* imaging of the breast cancer cells was done by fluorescence microscopy and fluorescence-activated cell sorting analysis. The *in vivo* images of breast tumors by NIR fluorescence and T_2-weighted MRI showed successful cellular uptake. Thus MQQ-probes have shown potential as imaging agents for *in vitro* and *in vivo* characterization of cancer tumors.

Wang *et al.* [140] developed a Rose Bengal conjugated gold nanorod (RB-GNR) system for optical detection of cancer cells. This system modified by poly (allylamine hydrochloride) exhibited strong optical absorption in the NIR region, good stability in aqueous solution, low cytotoxicity, and high specificity to oral cancer cells. The RB-GNR sensing probe was specifically conjugated with the oral cancer cells and their NIR absorption was monitored for specific, rapid and quantitative analysis of the oral cancer cell lysate.

Single cell studies

An effective cellular imaging method is required to track and monitor cellular/molecular events in the living organism. Lee *et al.* showed that the surface enhanced Raman scattering (SERS) can be used to monitor the cellular uptake of isocyanide functionalized silver and gold nanoparticles inside a single mammalian cell [141]. These nanoparticles show potential for monitoring and imaging the biological processes at the single cell level.

Optical nanoprobe of gold nanoparticles (size around 5 nm) coated with green fluorescent protein (GFP) nanobodies was used for non-invasive long-term single particle tracking [142]. These nanoprobes could be used both *in vitro* and *in vivo* and labeling both surface and intracellular GFP - protein in very crowded environments. They also provide complete information about the distribution of live or fixed cells by high density labeling. Due to small size of these probes, they have perfect photostability, high specificity, and versatility. They can be used to target nuclear proteins and also for correlative studies between optical and electron microscopy, as small gold nanoparticles provide high contrasts for both modalities [142].

In another approach, a carbon nanotube was attached to the tip of a glass micropipet to interrogate cells down to the single organelle level [143]. Yan *et al.* showed that a nanowire attached to the tip of an optical fiber could detect the optical signals from subcellular regions [144]. Actis *et al.* fabricated carbon nanoelectrodes using a topdown approach [145]. The nanoelectrode was functionalized with platinum to monitor oxygen consumption in the brain. They were also used for electrochemical measurements within the cell with minimal disturbance to cell function. These probes could be used as scanning ion conductance microscopy probes for high resolution electrochemical mapping of species in living cells.

Tumor microenvironment sensing

The tumor microenvironment plays a significant role in tumor development and metastasis. Tumor microenvironment features such as hypoxia, and overexpressed proteases differ significantly from those of normal tissues. These features can serve as both biomarkers for tumor diagnosis and theraputic targets for tumor treatment. Optical imaging techniques such as PET and magnetic resonance imaging (MRI) have been used to investigate the tumor microenvironment. Various imaging probes are well developed to target pH, hypoxia and proteases in the tumor microenvironment.

Construction of probes that target the tumor microenvironment via non-invasive imaging is of great interest to researchers [146-149]. A wide variety of nanoparticle systems currently are being developed for the construction of molecular imaging probes targeting the tumor microenvironment [9]. Nanoparticles such as the pH-titratable SPIOs have shown improved nanoparticle accumulation in acidic tumors [146]. The influence of an external magnet on a liposome containing clusters of magnetic nanoparticles can be used to target the tumor microenvironment and give high contrast MRI [150]. Receptor-ligand interactions are frequently used to generate nanoprobes to target the tumor microenvironment [151-153]. Fluorescent "smart" probes with special features can be used for optical imaging of the tumor microenvironment apart from conventional MRI and PET imaging [154].

Fluorescent nanorods and nanospheres are useful for real-time *in vivo* probing of nanoparticle shape-dependent tumor penetration [155]. Compared to small molecular probes, fluorescence nanoprobes offer advantages such as tunable circulation lifetime, systematic accumulation in the tumor and enhanced sensitivity due to tagging of multiple imaging molecules on a single nanoparticle. The mechanisms underlying pH responsive fluorescence of the nanoprobes include the FRET effect on the self-aggregation associated energy transfer (SAET) [156] effect. QDs have been used as FRET donors in pH nanoprobes. QD-dopamine-peptides can bioconjugate to develop a charge-transfer coupled pH probe [157]. The response of the QD conjugates to pH can be monitored by changes in the intrinsic redox properties of the coated dopamine upon oxidation at basic pH. QDs act as a donor in ratiometric pH probes which are based on FRET pairs. Organic dyes that respond to pH changes, such as fluorescein isothiocyanate (FITC), the pH dye SNARF and fluorescent diblock copolymers have been coated onto the surface of QDs to generate QD-based ratiometric pH probes [158-160]. QDs coated with pH-sensitive fluorescent proteins were recently reported to have dramatically improved sensitivity and photostability compared to the widely used fluorescent dyes for pH imaging [161]. In another study, dextran based pH-sensitive NIR nanoprobe were used for the *in vivo* differential-absorption dual-wavelength photoacoustic imaging of tumors [162]. Novel quantum dot nanoprobes were prepared and investigated for intracellular delivery and real-time imaging of siRNA [163,164].

In 2010, *Li et al.* [165] fabricated a highly sensitive nanoprobe lnNP1 to visualize human glioblastoma U87MG cancer cells *in vitro* and subcutaneous U87MG xenografts *in vivo* by pH-activated NRI fluorescence. Zhou *et al.* [166] described a set of tunable, pH-activatable micellar nanoprobes based on the supramolecular self-assembly of ionizable block copolymer micelles as a SAET-type pH nanoprobe (Figure 10a). Using amine groups with different pKa in the polymer backbone (Figure 10b), a series of SAET probes was obtained. These probes could be activated at different pH values because only the protonated ammonium groups would cause micelles to dissociate into unimers with a dramatic increase in fluorescence emission. Specific activation of nanoprobes in acidic tumor cells is shown in Figure 6c. A multicolored, pH tunable fluorescent nanoplatform was developed using the same principle using commonly available pH-insensitive dyes [167]. The fluorescence wavelengths could be fine-tuned from green to the NIR emission range (500-820 nm) on the nanoplatform and their fluorescence ON/OFF activation could be achieved within 0.25 pH units.

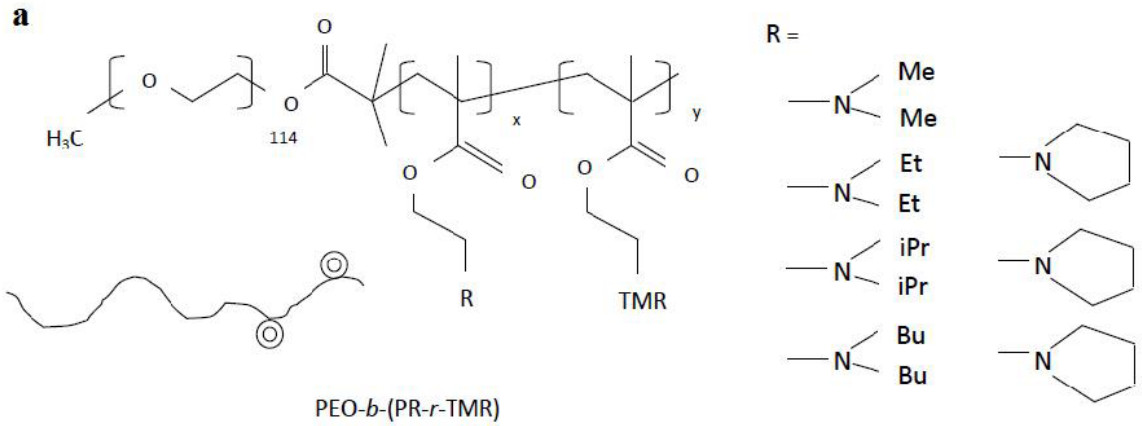

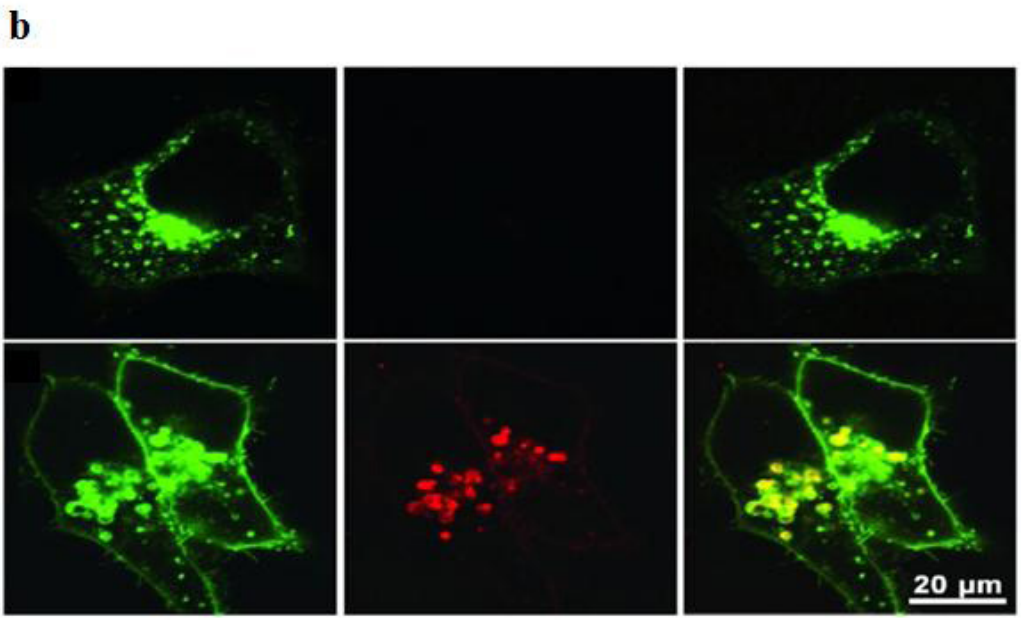

Figure 10: a) Formation of activatable nanoprobes by attaching different amine groups to the micelle backbone at different pH values upon protonation of the amine group; **b)** Fluorescent images of cells treated with pH-activatable nanoprobes with (top panel) or without (bottom panel) the inhibition of lysosomal acidification. Nanoprobe activation is indicated by the red fluorescence signals; Adapted from Zhou [166]

In addition to quantum dots and polymeric NPs, newly emerging nanomaterials been used to construct pH nanoprobes. For example, Shi *et al*. used a carbon nanodots (CDs) based ratiometric pH probe for quantitative measurement of the intracellular pH in the whole cell [168]. Figure 11a shows the amino-coated CDs. They were coated with different molar ratios of pH-sensitive FITC and to pH insensitive rhodamine B isothiocyanate (RBITC). Due to dual labeling of the CDs, the pH response range could be well adjusted (Figure 11b) [168]. They also showed good biocompatibility and intracellular dispersity. Such pH nanoprobes can be very useful for ratiometric imaging of the tumor microenvironment *in vivo.*

Also, small fluorescent probes when conjugated with nanoparticles showed improved biocompatibility and delivery efficiency with desirable emission range. Therefore, pH sensitive small molecule dyes conjugated to nanoprobes can be used for optical imaging of tumor microenvironment [169]. The specificity may be realized by attaching target groups onto the surface of nanoprobes. Some of the problems with these probes are narrow pH range and high uptake by kidney and liver cells during *in vivo* imaging. Further development of biocompatible nanocarriers and other pH nanoprobes is required to solve these problems.

Gold nanoparticles have been attractive contrast agents for cancer therapy, particularly their high-atomic number and biocompatibility. They could enhance secondary electron production as well as particles smaller than 100 nm can also cross human cell membranes and preferentially accumulate in cancer cells [170,171]. In a recent study, gold nanoparticles were found to increase survival rate of mice in conjunction with kilovoltage radiotherapy with EMT-6 mammary tumors to 86%, compared to 20% with radiotherapy alone [172]. Gold-iron oxide nanoparticles were demonstrated as dual - therapy and diagnostic applications. Laser assisted therapy and MRI based imaging showed selective accumulation of nanoparticles in SW1222 xenograft tumors [173]. Both cell killing and detection of tumor was possible.

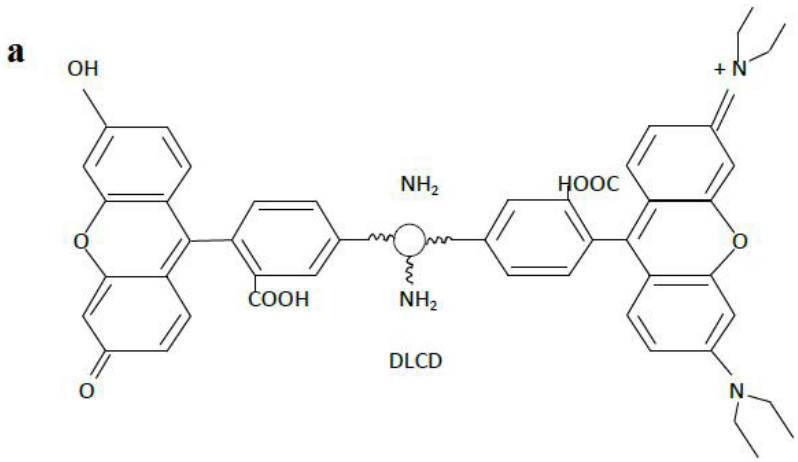

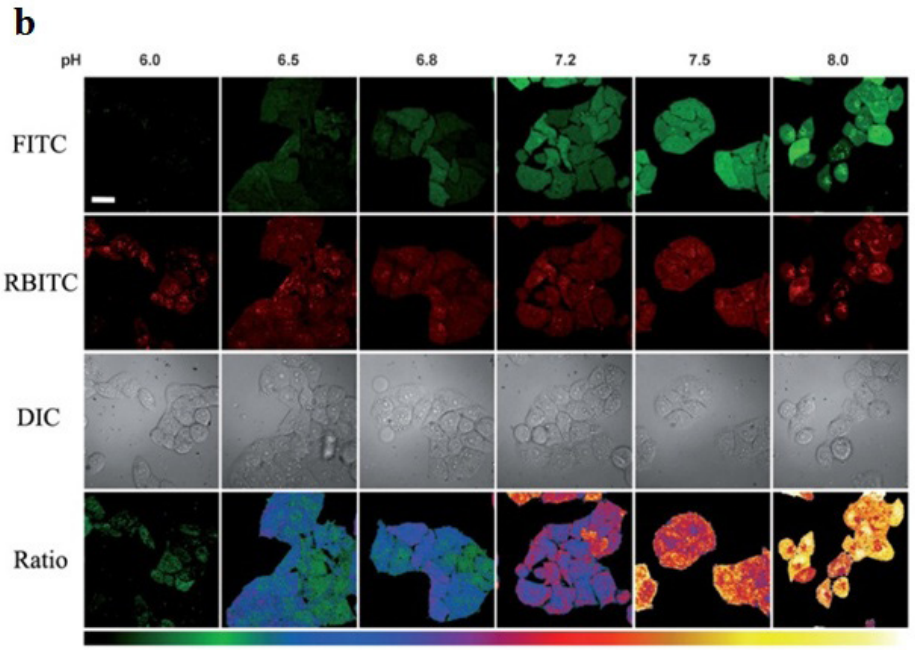

Figure 11: a) Structure of the dual-labeled carbon nanodot as ratiometric pH nanoprobe; **b)** Fluorescent images of HeLa cells at pH 6.0, 6.5, 6.8, 7.2, 7.5 and 8.0, respectively [168]

Several alloy based nanoparticles, such as copper-64-alloyed gold nanoparticles were used for cancer imaging [174]. The specific radioactivity of the alloyed gold nanoparticles could be freely and precisely controlled by the addition of the precursor (64) $CuCl_2$ to afford sensitive detection. The direct incorporation of (64) Cu into the lattice of the gold nanoparticle structure ensured the radiolabel stability for accurate localization *in vivo*. In another work Au-Fe alloy nanoparticles were designed for multimodal constrast agents [175]. Iron carbide Fe_5C_2 was prepared and used as MR contrast probe [176]. They possessed close-to bulk magnetization, small and tunable size (< 25 nm), narrow size distribution, and good colloidal stability. They were found to accumulate in tumors and induce more prominent signal change.

Nitric oxide detection

Nitric oxide (NO) has a significant role in blood-pressure regulation and neurotransmission [177]. In endothelial cells, neurons and astrocytes, NO is synthesized from L-arginine in a reaction catalyzed by nitric oxide synthase (NOS) [178]. Gil *et al.* [179] developed an optical sensor for determination of intracellular NO which were prepared by depositing gold nanoparticles on polymer beads coated with mesoporous silica and followed by calcination. There was an increase in concentration of plasmonic material per sensing particle and hence showed improved biocompatibility and and a better signal-to-noise ratio. These sensors could possibly reside inside cells and detect multiple analytes.

Peroxynitrite ($ONOO^-$) is a highly reactive species and involved in studies of several diseases. Fluorescent probes have been designed to selectively detect $ONOO^-$ in living cells. Tian *et al.* [180] developed a fluorescent nanoprobe based on a polymeric micelle and coated with cell-penetrating peptide. The ratiometric detection and imaging of $ONOO^-$ is done by a nanoprobe which made up of $ONOO^-$ indicator dye and reference dye. The nanoprobe is not influenced by enzymatic reactions and high-concentrations of OH and ClO^-. This nanoprobe also has good water solubility, photostability, biocompatibility, and NIR excitation and emission. Confocal microscopy was used to visualize $ONOO^-$ in living cells with the nanoprobe. They also exhibits very low toxicity and good membrane permeability.

Angiogenic vasculature

Angiogenesis is the primitive cause of tumor, growth, metastasis and invasion of tumors [181-184]. Vascular endothelial growth factor (VEGF) and receptor (VEGFR) signaling pathway promote tumor-induced angiogenesis [181,182].

Karathanasis *et al.* [185] developed a 100 nm imaging nanoprobe that was deposited inside the tumor and mammography was used to measure the tumor vascular permeability in a rat MAT B III breast tumor model. The tumor vascular permeability varied widely among the animals. A qRT-PCR was used to measure VEGF and VEGF receptor-2 gene expression of the tumors. They showed strong correlation with that of the nanoproble while measuring the vascular permeability which widely varied among animals. High intra tumoral deposition of nanoscale agent was found at high angiogenic activity could be correlated with faster tumor growth rate.

Nucleic acid-based aptamers was developed for delivering diagnostic nanoprobes at specific locations. Kim *et al.* [186] developed a new class of smart imaging nanoprobe for specific detection of the angiogenic vasculature of glioblastoma using MRI. It was made up of a magnetic nanocrystal imaging core. The thermal decomposition method was used to synthesize the core and surface

was functionalized by carboxyl polysorbate 80 to enhance water solubilization and conjugation of the targeting moiety. Amine-functionalized aptamers were conjugated to the carboxylated magnetic nanosrystal that specifically bind to the VEGFR2. When tested *in vivo* they could effectively target VEGFR2, showed excellent MRI sensitivity and no cytotoxicity.

Kessinger *et al*. [187] developed an an $\alpha_v\beta_3$-specific nanoprobe consisting of fluorescent superparamagnetic polymeric micelles (FSPPM) and used in *in vivo* imaging of tumor angiogenesis. Spherical micelles of poly(ethylene glycol)-*b*-poly(D,L-lactide) co-polymers conjugated with the fluorescent dye tetramethylrhodamine, were loaded with SPIO NPs. The resulting micelle diameter was determined to be 50–70 nm based on dynamic light scattering and transmission electron microscopy measurements. Micelles were encoded with an $\alpha_v\beta_3$-specific peptide, cyclic RGDfK, and optimized for maximum fluorescence and targeting in $\alpha_v\beta_3$-overexpressing cells *in vitro*. In mice, cRGD-FSPPM-treated animals have shown $\alpha_v\beta_3$-specific FSPPM accumulation in human lung cancer subcutaneous tumor xenografts.

Current challenges in Nanoprobe development

Enormous opportunities for designing and developing sensitive nanoprobes for molecular imaging have emerged in recent years. The potential to diagnose and monitor several diseases in patients using nanoprobes has become possible in reality. However, there remain considerable challenges to applying these nanoprobes in humans. In addition to the purity, dispensability and stability of nanoprobes in physiological environments, the variable physicochemical properties of different nanoprobes might give unexpected results when tested *in vivo*. As discussed in this review, nanoprobes might be systemically distributed in organs and tissues. However, due to wide variation in the properties of nanomaterials, absorption, distribution, metabolism and excretion characteristics are highly variable for nanoprobes [188-190].

It may take many years for clinical adaptation of nanoprobe-based molecular imaging to occur as these probes generally undergo rigorous process of redesign, optimization and validation. Several issues need to be overcome before nanoprobes will be ready for clinical translation. For example, i) the starting materials to construct a nanoprobe must be biodegradable and biocompatible, ii) the synthesized nanoprobes must have high QY and a deep penetration ratio, iii) sufficient photostability is required, iv) an appropriate surface coating is needed to avoid non-specifiic binding during circulation or RES uptake, v) they need to be appropriate size and have a long half-life long enough for extravasation to occur, vi) they must have high specificity and selectivity and vii) they must be multimodal and multifunctional. Apart from the imaging potential of these probes, the pharmacokinetics and toxicity should be investigated. FDA approved, biodegradable and biocompatible materials are usually considered as good starting materials for fabricating nanoprobes. Although imaging of tumors using nanoprobes is successful in small animal models, further investigation is required to study unfavorable biodistribution and nonspecific accumulation of these probes. The major challenge is to encapsulate or biofunctionalize the nanoprobe such that it can escape from the RES and also conjugate to specific targeting molecules. Innovations in preparation of nanoprobes for imaging of deep tissues with high QY and deep tissue penetration are also needed. The important clinical applications of nanoprobes will be imaging tissues close to skin. The use of multifunctional nanoparticles would provide tumor assessment ability and intraoperative surgical guidance for tumor tissue resection [191,192].

Conclusion and Future Perspective

For many diseases, early detection is critical component to improving a patient's survival. The development of new imaging systems and imaging agents has significantly improved the ability to detect disease earlier in it progression. Nanoprobes have immense potential to increase the sensitivity and specificity of imaging systems. Though these probes have several advantages, the most important concern is the toxicity of these probes as these nanomaterials are made of metallic or inorganic components. However, clinical applications of nanoprobes in diagnosis of liver lesions and cancer metastases in lymph nodes are available. There should be clinical nanoprobes to target more metastatic sites such as brain and bones. Further investigation regarding the synthesis and interaction between the nanomaterials and the tissues in the body will lead to possible design of safer nanoprobes. Another promising application of nanoprobes is as theranostic agents that combine imaging and therapeutic modalities. Advanced designs of nanoprobes and theranostic agents are anticipated to significantly improve patient care and compliance. There is a huge potential of discovering novel agents with advanced and more efficient properties by combining multidisciplinary areas such as chemistry, bioengineering, toxicology and clinical research.

Acknowledgement

This work was supported by RIG, BITS Pilani and UGC, New Delhi.

References

1. Wu HF, Agrawal K, Shrivas K, Lee YH (2010) On particle ionization/enrichment of multifunctional nanoprobes: washing/separation-free, acceleration and enrichment of microwave-assisted tryptic digestion of proteins via bare TiO2 nanoparticles in ESI-MS and comparing to MALDI-MS. J Mass Spectrom 45: 1402-8.

2. Khandelwal P, Beyer CE, Lin Q, Schechter LE, Bach AC (2004) Studying Rat Brain Neurochemistry Using Nanoprobe NMR Spectroscopy: a Metabonomics Approach. Analyt Chem 76: 4123-7.

3. Panchapakesan B, Book-Newell, Brittany, Sethu Palaniappan, Rao M, Irudayaraj J (2011) Gold nanoprobes for theranostics. Nanomedicine 6: 1787-811.

4. Xu JJ, Zhao WW, Song S, Fan C, Chen HY (2014) Functional nanoprobes for ultrasensitive detection of biomolecules: an update. Chemical Society Reviews 43: 1601-11.

5. Harris S, Duke-designed nanoprobes may detect early disease markers. News and observer Science & Technology.

6. Johnson L, Spence TZ Michelle (2010) Fluorescence fundamentals. In Molecular Probes Handbook, A Guide to Fluorescent Probes and Labeling Technologies, 2010.

7. Weissleder R (2002) Scaling down imaging: Molecular mapping of cancer in mice. Nat Rev Cancer 2: 11-8.

8. Escobedo JO, Rusin O, Lim S, Strongin RM (2010) NIR dyes for bioimaging applications. Current Opinion in Chemical Biology 14: 64.

9. He X, Gao J, Gambhir SS, Cheng Z (2010) Near-infrared fluorescent nanoprobes for cancer molecular imaging: status and challenges. Trends in Mol Med 16: 574-83.

10. Luo S, Zhang E, Su Y, Cheng T, Shi C (2011) A review of NIR dyes in cancer targeting and imaging. Biomaterials 32: 7127-38.

11. Achilefu S (2010) The Insatiable Quest for Near-Infrared Fluorescent Probes for Molecular Imaging. Angew Chem Int Ed Engl 49: 9816-8.

12. Wu C, Bull B, Szymanski C, Christensen K, McNeill J (2008) Multicolor Conjugated Polymer Dots for Biological Fluorescence Imaging. ACS Nano 2: 2415-23.

13. Yang Y, An F, Liu Z, Zhang X, Zhou M, et al. (2012) Ultrabright and ultrastable near-infrared dye nanoparticles for in vitro and in vivo bioimaging. Biomaterials 33: 7803-9.

14. Parthasarathy V, Fery-Forgues S, Campioli E, Recher G, Terenziani F, et al. (2011) Dipolar versus Octupolar Triphenylamine-Based Fluorescent Organic Nanoparticles as Brilliant One- and Two-Photon Emitters for (Bio)imaging. Small 7: 3219-29.

15. An BK, Kwon SK, Jung SD, Park SY (2002) Enhanced Emission and Its Switching in Fluorescent Organic Nanoparticles. J Am Chem Soc 124: 14410-5.

16. Yu J, Zhang X, Hao X, Zhang X, Zhou M, et al. (2014) Near-infrared fluorescence imaging using organic dye nanoparticles. Biomaterials 35: 3356-64.

17. Yang S, Lu D, Tian L, He F, Chen G, et al. (2011) Stable water-dispersed organic nanoparticles: preparation, optical properties, and cell imaging application. Nanoscale 3: 2261-7.

18. Gao F, Liao Q, Xu ZZ, Yue YH, Wang Q, et al. (2010) Strong Two-Photon Excited Fluorescence and Stimulated Emission from an Organic Single Crystal of an Oligo(Phenylene Vinylene). Angewandte Chemie Int Ed 49: 732-5.

19. Seferos DS, Banach DA, Alcantar NA, Israelachvili JN, Bazan GC (2004) α,ω-Bis(thioacetyl)oligophenylenevinylene Chromophores from Thioanisol Precursors. J Org Chem 69: 1110-9.

20. Adams KE, Ke S, Kwon S, Liang F, Fan Z, et al. (2007) Comparison of visible and near-infrared wavelength-excitable fluorescent dyes for molecular imaging of cancer. J Biomed Opt 12: 024017.

21. Benson RC, Kues HA (1978) Fluorescence properties of indocyanine green as related to angiography. Phys Med Biol 23: 159-63.

22. Weissleder R (2001) Clearer vision for in vivo imaging. Nat Biotechnol 19: 316-7.

23. Malicka J, Gryczynski I, Geddes CD, Lakowicz JR (2003) Metal-enhanced emission from indocyanine green: a new approach to in vivo imaging. J Biomed Opt 8: 472-8.

24. Yu J, Yaseen MA, Anvari B, Wong MS (2007) Synthesis of Near-Infrared-Absorbing Nanoparticle-Assembled Capsules. Chem Mater 19: 1277-84.

25. Maarek JM, Holschneider DP, Harimoto J (2001) Fluorescence of indocyanine green in blood: intensity dependence on concentration and stabilization with sodium polyaspartate. J Photochem Photobiol B 65: 157-64.

26. Zheng C, Zheng M, Gong P, Jia D, Zhang P, et al. (2012) Indocyanine green-loaded biodegradable tumor targeting nanoprobes for in vitro and in vivo imaging. Biomaterials 33: 5603-9.

27. Yue C, Liu P, Zheng M, Zhao P, Wang Y, et al. (2013) IR-780 dye loaded tumor targeting theranostic nanoparticles for NIR imaging and photothermal therapy. Biomaterials 34: 6853-61.

28. Yang Y, Xiang K, Yang YX, Wang YW, Zhang X, et al. (2013) An individually coated near-infrared fluorescent protein as a safe and robust nanoprobe for in vivo imaging. Nanoscale 5: 10345-52.

29. Luo H, Yang J, Jin H, Huang C, Fu J, et al. (2011) Tetrameric far-red fluorescent protein as a scaffold to assemble an octavalent peptide nanoprobe for enhanced tumor targeting and intracellular uptake in vivo. The FASEB J 25: 1865-73.

30. Donner J, Thompson S, Kreuzer M, Baffou G, Quidant R (2012) Mapping intracellular temperature using Green fluorescent Protein. Nanoletters 12: 2107-11.

31. Minard-Basquin C, Weil T, Hohner A, Rädler JO, Müllen KA (2013) Polyphenylene Dendrimer–Detergent Complex as a Highly Fluorescent Probe for Bioassays. J Am Chem Soc 125: 5832-8.

32. Oesterling I, Müllen K (2007) Multichromophoric Polyphenylene Dendrimers: Toward Brilliant Light Emitters with an Increased Number of Fluorophores. J Am Chem Soc 129: 4595-605.

33. Fei X, Gu Y, Lan Y, Shi B (2011) Fluorescent properties of novel dendrimer dyes based on thiazole orange. J Luminescence 131: 2148-52.

34. Talanov VS, Regino CA, Kobayashi H, Bernardo M, Choyke PL, et al. (2006) Dendrimer-Based Nanoprobe for Dual Modality Magnetic Resonance and Fluorescence Imaging. Nano Letters 6: 1459-63.

35. Kim Y, Kim Sung H, Tanyeri M, Katzenellenbogen John A, Schroeder Charles M (2013) Dendrimer Probes for Enhanced Photostability and Localization in Fluorescence Imaging. Biophys J 104: 1566-75.

36. Almutairi A, Guillaudeu SJ, Berezin MY, Achilefu S, Frechet JMJ (2008) Biodegradable pH-sensing dendritic nanoprobes for Near-Infrared Fluorescence Lifetime and Intensity Imaging. J Am Chem Soc 130: 444-5.

37. Bruchez M, Moronne M, Gin P, Weiss S, Alivisatos AP (1998) Semiconductor Nanocrystals as Fluorescent Biological Labels. Science 281: 2013-6.

38. Mazumder S, Dey R, Mitra MK, Mukherjee S, Das GC (2009) Review: Biofunctionalized Quantum Dots in Biology and Medicine. J Nanomat 2009.

39. Mérian J, Gravier J, Navarro F, Texier I (2012) Fluorescent Nanoprobes Dedicated to in Vivo Imaging: From Preclinical Validations to Clinical Translation. Molecules 17: 5564-91.

40. Li ZF, Ruckenstein E (2004) Water-Soluble Poly(acrylic acid) Grafted Luminescent Silicon Nanoparticles and Their Use as Fluorescent Biological Staining Labels. Nano Letters 4: 1463-7.

41. Park JH, Gu Luo, von Maltzahn, Geoffrey Ruoslahti, Erkki Bhatia, et al. (2009) Biodegradable luminescent porous silicon nanoparticles for in vivo applications. Nat Mater 8: 331-6.

42. Nurunnabi M, Cho KJ, Choi JS, Huh KM, Lee YK (2010) Targeted near-IR QDs-loaded micelles for cancer therapy and imaging. Biomaterials 31: 5436-44.

43. Liu Y, Ai K, Yuan Q, Lu L (2011) Fluorescence-enhanced gadolinium-doped zinc oxide quantum dots for magnetic resonance and fluorescence imaging. Biomaterials 32: 1185-92.

44. Generalova AN, Oleinikov VA, Sukhanova A, Artemyev MV, Zubov VP, et al. (2013) Quantum dot-containing polymer particles with thermosensitive fluorescence. Biosens Bioelectron 39: 187-93.

45. Sun Y, Balasubramanian K, Rao TUB, Pradeep T (2011) First Principles Studies of Two Luminescent Molecular Quantum Clusters of Silver, Ag7(H2MSA)7 and Ag8(H2MSA)8, Based on Experimental Fluorescence Spectra. J Phys Chem C 115: 20380-7.

46. Yuan X, Luo Z, Zhang Q, Zhang X, Zheng Y, et al. (2011) Synthesis of Highly Fluorescent Metal (Ag, Au, Pt, and Cu) Nanoclusters by Electrostatically Induced Reversible Phase Transfer. ACS Nano 5: 8800-8.

47. Selvam T, Chi KM (2011) Synthesis of hydrophobic gold nanoclusters: growth mechanism study, luminescence property and catalytic application. J Nanopart Res 13: 1769-80.

48. Devadas MS, Kim J, Sinn E, Lee D, Goodson T, et al. (2010) Unique Ultrafast Visible Luminescence in Monolayer-Protected Au25 Clusters. J Phys Chem C 114: 22417-23.

49. Wu Z, Jin R (2010) On the Ligand's Role in the Fluorescence of Gold Nanoclusters. Nano Letters 10: 2568-73.

50. Guo S, Wang E (2011) Noble metal nanomaterials: Controllable synthesis and application in fuel cells and analytical sensors. Nano Today 6: 240-64.

51. Zheng J, Nicovich, PR, Dickson RM (2007) Highly Fluorescent Noble-Metal Quantum Dots. Annu Rev Phys Chem 58: 409-31.

52. Shang L, Dong S (2009) Sensitive detection of cysteine based on fluorescent silver clusters. Biosens Bioelectron 24: 1569-73.

53. Huang CC, Chen CT, Shiang YC, Lin ZH, Chang HT (2009) Synthesis of Fluorescent Carbohydrate-Protected Au Nanodots for Detection of Concanavalin A and Escherichia coli. Analyt Chem 81: 875-82.

54. Wei H, Wang Z, Yang L, Tian S, Hou C, et al. (2010) Lysozyme-stabilized gold fluorescent cluster: Synthesis and application as Hg2+ sensor. Analyst 135: 1406-10.

55. Yu J, Patel SA, Dickson RM (2007) In Vitro and Intracellular Production of Peptide-Encapsulated Fluorescent Silver Nanoclusters. Angew Chem Int Ed Engl 46: 2028-30.

56. Richards CI, Choi S, Hsiang JC, Antoku Y, Vosch T, et al. (2008) Oligonucleotide-Stabilized Ag Nanocluster Fluorophores. J Am Chem Soc 130: 5038-9.

57. Yu J, Choi S, Dickson RM (2009) Shuttle-Based Fluorogenic Silver-Cluster Biolabels. Angew Chem Int Ed Engl. 48: 318-20.

58. Negishi Y, Takasugi Y, Sato S, Yao H, Kimura K, et al. (2004) Magic-Numbered Au Clusters Protected by Glutathione Monolayers (n = 18, 21, 25, 28, 32, 39): Isolation and Spectroscopic Characterization. J Am Chem Soc 126: 6518-9.

59. Negishi Y, Nobusada K, Tsukuda T (2005) Glutathione-Protected Gold Clusters Revisited: Bridging the Gap between Gold(I)−Thiolate Complexes and Thiolate-Protected Gold Nanocrystals. J Am Chem Soc 127: 5261-70.

60. Negishi Y, Chaki NK, Shichibu Y, Whetten RL, Tsukuda T (2007) Origin of Magic Stability of Thiolated Gold Clusters: A Case Study on Au25(SC6H13)18. J Am Chem Soc 129: 11322-3.

61. Wang G, Huang T, Murray RW, Menard L, Nuzzo RG (2004) Near-IR Luminescence of Monolayer-Protected Metal Clusters. J Am Chem Soc 127: 812-3.

62. Shichibu Y, Negishi Y, Tsunoyama H, Kanehara M, Teranishi T, et al. (2007 Extremely High Stability of Glutathionate-Protected Au25 Clusters Against Core Etching. Small 3: 835-9.

63. Jana NR, Peng X (2003) Single-Phase and Gram-Scale Routes toward Nearly Monodisperse Au and Other Noble Metal Nanocrystals. J Am Chem Soc 125: 14280-1.

64. Lin CAJ, Yang TY, Lee CH, Huang SH, Sperling RA, et al. (2009) Synthesis, Characterization, and Bioconjugation of Fluorescent Gold Nanoclusters toward Biological Labeling Applications. ACS Nano 3: 395-401.

65. Bao Y, Yeh HC, Zhong C, Ivanov SA, Sharma JK, et al. (2010) Formation and Stabilization of Fluorescent Gold Nanoclusters Using Small Molecules†. J Phy Chem C 114: 15879-82.

66. Xie J, Zheng Y, Ying JY (2009) Protein-Directed Synthesis of Highly Fluorescent Gold Nanoclusters. J Am Chem Soc 131: 888-9.

67. Wu X, He X, Wang K, Xie C, Zhou B, et al. (2010) Ultrasmall near-infrared gold nanoclusters for tumor fluorescence imaging in vivo. Nanoscale 2: 2244-9.

68. Koo V, Hamilton PW, Williamson K (2006) Non-invasive in vivo imaging in small animal research. Cell Oncol 28: 127-39.

69. Licha K, Olbrich C (2005) Optical imaging in drug discovery and diagnostic applications. Adv Drug Deliv Rev 57: 1087-108.

70. Lee H, Lee K, Kim IK, Park TG (2008) Synthesis, characterization, and in vivo diagnostic applications of hyaluronic acid immobilized gold nanoprobes. Biomaterials 29: 4709-18.

71. Wang H, Zheng L, Peng C, Shen M, Shi X, et al. (2013) Folic acid-modified dendrimer-entrapped gold nanoparticles as nanoprobes for targeted CT imaging of human lung adencarcinoma. Biomaterials 34: 470-80.

72. Zheng J, Petty JT, Dickson RM (2003) High quantum yield blue emission from water soluble Au8 nanodots. J Am Chem Soc 125: 7780-1.

73. Wilcoxon JP, Martin JE, Parsapour F, Wiedenman B, Kelley DF (1998) Photoluminescence from nanosize gold clusters. J Chem Phys 108: 9137-43.

74. Beversluis MR, Bouhelier A, Novotny L (2003) Continuum generation from single gold nanostructures through near-Field mediated intraband transitions. Phys Rev B: Condens Matter Mater Phys 68: 115433.

75. Wang M, Abbineni G, Clevenger A, Mao C, Xu S (2011) Upconversion nanoparticles: synthesis, surface modification and biological applications. Nanomedicine 7: 710-29.

76. Wu S, Han G, Milliron DJ, Aloni S, Altoe V, et al. (2009) Non-blinking and photostable upconverted luminescence from single lanthanide-doped nanocrystals. Procee Nat Acad Sci 106: 10917–21.

77. Li Z, Zhang Y, Jiang S (2008) Multicolor Core/Shell-Structured Upconversion Fluorescent Nanoparticles. Adv Mater 20: 4765-9.

78. Liu Q, Sun Y, Yang T, Feng W, Li C, et al. (2011) Sub-10 nm Hexagonal Lanthanide-Doped NaLuF4 Upconversion Nanocrystals for Sensitive Bioimaging in Vivo. J Am Chem Soc 133: 17122-5.

79. Auzel F (2003) Upconversion and Anti-Stokes Processes with f and d Ions in Solids. Chem Rev 104: 139-74.

80. Wang F, Liu X (2009) Recent advances in the chemistry of lanthanide-doped upconversion nanocrystals. Chem Soc Rev 38: 976-89.

81. Wang F, Banerjee D, Liu Y, Chen X, Liu X (2010) Upconversion nanoparticles in biological labeling, imaging, and therapy. Analyst 135: 1839-54.

82. Haase M, Schäfer H (2011) Upconverting Nanoparticles. Angew Chem Int Ed Engl 50: 5808-829.

83. Chen G, Qiu H, Prasad PN, Chen X (2014) Upconversion Nanoparticles: Design, Nanochemistry, and Applications in Theranostics. Chem Rev 114: 5161-214.

84. Yu XF, Sun Z, Li M, Xiang Y, Wang QQ, et al. (2010) Neurotoxin-conjugated upconversion nanoprobes for direct visualization of tumors under near-infrared irradiation. Biomaterials 31: 8724-31.

85. Liu Jn, Bu W, Pan Lm, Zhang S, Chen F, et al. (2012) Simultaneous nuclear imaging and intranuclear drug delivery by nuclear-targeted multifunctional upconversion nanoprobes. Biomaterials 33: 7282-90.

86. Zeng S, Tsang MK, Chan CF, Wong KL, Hao J (2012) PEG modified BaGdF5:Yb/Er nanoprobes for multi-modal upconversion fluorescent, in vivo X-ray computed tomography and biomagnetic imaging. Biomaterials 33: 9232-8.

87. Liu Z, Ju E, Liu J, Du Y, Li Z, et al. (2013) Direct visualization of gastrointestinal tract with lanthanide-doped BaYbF5 upconversion nanoprobes. Biomaterials 34: 7444-52.

88. Wang Y, Wang H, Liu D, Song S, Wang X, et al. (2013) Graphene oxide covalently grafted upconversion nanoparticles for combined NIR mediated imaging and photothermal/photodynamic cancer therapy. Biomaterials 34: 7715-24.

89. Thorek DJ, Chen A, Czupryna J, Tsourkas A (2006) Superparamagnetic Iron Oxide Nanoparticle Probes for Molecular Imaging. Ann Biomed Eng 34: 23-38.

90. Belin T, Guigue-Millot N, Caillot T, Aymes D, Niepce JC (2002) Influence of Grain Size, Oxygen Stoichiometry, and Synthesis Conditions on the γ-Fe2O3 Vacancies Ordering and Lattice Parameters. J Solid State Chem 163: 459-65.

91. Cornell RM, U Schertmann (1996) The Iron Oxides: Structure, Properties, Reactions, Occurrence and Uses. Weinheim : VCH Publishers: 1996.

92. Tebble RS, DJ Craik (1969) Magnetic Materials. Wiley-Interscience: London, 1969.

93. Massart R, Dubois E, Cabuil V, Hasmonay E (1995) Preparation and properties of monodisperse magnetic fluids. J Magnetism Magnet Mater 149: 1-5.

94. Hinds KA, Hill JM, Shapiro EM, Laukkanen MO, Silva AC, et al. (2003) Highly efficient endosomal labeling of progenitor and stem cells with large magnetic particles allows magnetic resonance imaging of single cells. Blood 102: 867-72.

95. Shapiro EM, Skrtic S, Sharer K, Hill JM, Dunbar CE, et al. (2004) MRI detection of single particles for cellular imaging. Procee Nat Acad Sci United States America 101: 10901-6.

96. Kemsheadl JT, Ugelstad J (1985) Magnetic separation techniques: their application to medicine. Mol Cell Biochem 67: 11-8.

97. Fabry B, Maksym GN, Butler JP, Glogauer M, Navajas D, et al. (2001) Scaling the Microrheology of Living Cells. Phys Rev Lett 87: 148102.

98. Wang N, Butler J, Ingber D (1993) Mechanotransduction across the cell surface and through the cytoskeleton. Science 260: 1124-7.

99. Hahn PF, Stark DD, Lewis JM, Saini S, Elizondo G, et al. (1990) First clinical trial of a new superparamagnetic iron oxide for use as an oral gastrointestinal contrast agent in MR imaging. Radiology 175: 695-700.

100. Pankhurst QA, Connolly J, Jones SK, Dobson J (2003) Applications of magnetic nanoparticles in biomedicine. J Phys D: Appl Phys 36: 167-81.

101. Liu G, Wang Z, Lu J, Xia C, Gao F, et al. (2011) Low molecular weight alkyl-polycation wrapped magnetite nanoparticle clusters as MRI probes for stem cell labeling and in vivo imaging. Biomaterials 32: 528-37.

102. Hildebrandt N, Hermsdorf Dana, Sign Orell, Ruth Schmitz SA, Diederichsen U (2007) Superparamagnetic iron oxide nanoparticles functionalized with peptides by electrostatic interactions. ARKIVOC 2007: 79-90.

103. Ferrucci JT, Stark DD (1990) Iron oxide-enhanced MR imaging of the liver and spleen: review of the first 5 years. AJR Am J Roentgenolo 155: 943-50.

104. Mahfouz AE, Taupitz M (1997) Contrast agents for MR imaging of the liver: a clinical overview. Eur Radiol 7: 507-13.

105. Wong SS, Woolley AT, Odom TW, Huang JL, Kim P, et al. (1998) Single-walled carbon nanotube probes for high-resolution nanostructure imaging. Applied Physics Letter 73: 3465-7.

106. Welsher K, Liu Z, Daranciang D, Dai H (2008) Selective Probing and Imaging of Cells with Single Walled Carbon Nanotubes as Near-Infrared Fluorescent Molecules. Nano Lett 8: 586-90.

107. Miki K, Oride K, Inoue S, Kuramochi Y, Nayak RR, et al. (2010) Ring-opening metathesis polymerization-based synthesis of polymeric nanoparticles for enhanced tumor imaging in vivo: Synergistic effect of folate-receptor targeting and PEGylation. Biomaterials 31: 934-42.

108. Saxena V, Sadoqi M, Shao J (2004) Enhanced photo-stability, thermal-stability and aqueous-stability of indocyanine green in polymeric nanoparticulate systems. J Photochem Photobiol B 74: 29-38.

109. Saxena V, Sadoqi M, Shao J (2006) Polymeric nanoparticulate delivery system for Indocyanine green: Biodistribution in healthy mice. Int J Pharma 308: 200-4.

110. Larush L, Magdassi S (2011) Formation of near-infrared fluorescent nanoparticles for medical imaging. Nanomedicine 6: 233-40.

111. Schädlich A, Rose C, Kuntsche J, Caysa H, Mueller T, et al. (2011) How Stealthy are PEG-PLA Nanoparticles? An NIR In Vivo Study Combined with Detailed Size Measurements. Pharma Res 28: 1995-2007.

112. Tong R, Coyle VJ, Tang L, Barger AM, Fan TM, et al. (2010) Polylactide nanoparticles containing stably incorporated cyanine dyes for in vitro and in vivo imaging applications. Microsc Res Tech 73: 901-9.

113. Longmire MR, Ogawa M, Choyke PL, Kobayashi H (2011) Biologically Optimized Nanosized Molecules and Particles: More than Just Size. Bioconjug Chem 22: 993-1000.

114. Almutairi A, Akers WJ, Berezin MY, Achilefu S, Fréchet JM (2008) Monitoring the Biodegradation of Dendritic Near-Infrared Nanoprobes by in Vivo Fluorescence Imaging. Mol Pharma 5: 1103-10.

115. Quadir MA, Radowski MR, Kratz F, Licha K, Hauff P, et al. (2008) Dendritic multishell architectures for drug and dye transport. J Control Release 132: 289-94.

116. Lin X, Konno T, Ishihara K (2013) Cell-Membrane-Permeable and Cytocompatible Phospholipid Polymer Nanoprobes Conjugated with Molecular Beacons. Biomacromolecules 15: 150-7.

117. Kim WJ, Bonoiu AC, Hayakawa T, Xia C, Kakimoto MA, et al. (2009) Hyperbranched polysiloxysilane nanoparticles: Surface charge control of nonviral gene delivery vectors and nanoprobes. Int J Pharm 376: 141-52.

118. Barenholz Y, Crommelin DJA (1994) Liposomes as a pharmaceutical dosage forms In: Encyclopedia of Pharmaceutical Technology, Vol. 9, Taylor & Francis Publisher, USA.

119. Torchilin VP (2005) Recent advances with liposomes as pharmaceutical carriers. Nat Rev Drug Discov 4: 145-60.

120. Pastorino F, Brignole C, Marimpietri D, Sapra P, Moase EH, et al. (2003) Doxorubicin-loaded Fab´ Fragments of Anti-disialoganglioside Immunoliposomes Selectively Inhibit the Growth and Dissemination of Human Neuroblastoma in Nude Mice. Cancer Res 63: 86-92.

121. Klibanov AL, Maruyama K, Torchilin VP, Huang L (1990) Amphipathic polyethyleneglycols effectively prolong the circulation time of liposomes. FEBS Lett 268: 235-7.

122. Gabizon AA (2001) Pegylated Liposomal Doxorubicin: Metamorphosis of an Old Drug into a New Form of Chemotherapy. Cancer Invest 19: 424-36.

123. Zhang L, Zhao D (2013) Liposomal Encapsulation Enhances In Vivo Near Infrared Imaging of Exposed Phosphatidylserine in a Mouse Glioma Model. Molecules 18: 14613-28.

124. Portnoy E, Lecht S, Lazarovici P, Danino D, Magdassi S (2011) Cetuximab-labeled liposomes containing near-infrared probe for in vivo imaging. Nanomedicine 7: 480-8.

125. Gao X, Li C (2014) Nanoprobes Visualizing Gliomas by Crossing the Blood Brain Tumor Barrier. Small 10: 426-40.

126. Brambilla D, Verpillot R, Le Droumaguet B, Nicolas J, Taverna M, et al. (2012) PEGylated Nanoparticles Bind to and Alter Amyloid-Beta Peptide Conformation: Toward Engineering of Functional Nanomedicines for Alzheimer's Disease. ACS Nano 6: 5897-908.

127. Wiesehan K, Stöhr J, Nagel-Steger L, van Groen T, Riesner D, et al. (2008) Inhibition of cytotoxicity and amyloid fibril formation by a d-amino acid peptide that specifically binds to Alzheimer's disease amyloid peptide. Protein Eng Des Sel 21: 241-6.

128. Zhang C, Wan X, Zheng X, Shao X, Liu Q, et al. (2014) Dual-functional nanoparticles targeting amyloid plaques in the brains of Alzheimer's disease mice. Biomaterials 35: 456-65.

129. Jaruszewski KM, Curran GL, Swaminathan SK, Rosenberg JT, Grant SC, et al. (2014) Multimodal Nanoprobes to target cerebrovascular amyloid in Alzheimer's disease brain. Biomaterials 35: 1967-76.

130. Sun C, Veiseh O, Gunn J, Fang C, Hansen S, et al. (2008) In Vivo MRI Detection of Gliomas by Chlorotoxin-Conjugated Superparamagnetic Nanoprobes. Small 4: 372-9.

131. Hoskins WJ (1995) Prospective on ovarian cancer: Why prevent? J Cell Biochem 59: 189-99.

132. Society AC (2011) Cancer facts & figures. American Cancer Society: GA: Atlanta, 2011.

133. Xi L, Satpathy M, Zhao Q, Qian W, Yang L, et al. (2014) Jiang H HER-2/neu targeted delivery of a nanoprobe enables dual photoacoustic and fluorescence tomography of ovarian cancer. Nanomedicine 10: 669-77.

134. Alitalo K (2011) The lymphatic vasculature in disease. Nat Med 17: 1371-80.

135. Tammela T, Alitalo K (2010) Lymphangiogenesis: Molecular Mechanisms and Future Promise. Cell 140: 460-76.

136. Achen MG, McColl BK, Stacker SA (2005) Focus on lymphangiogenesis in tumor metastasis. Cancer Cell 7: 121-7.

137. Alex JC, Krag DN (1993) Gamma-probe guided localization of lymph nodes. Surgical Oncology 2: 137-43.

138. Huang X, Zhang F, Lee S, Swierczewska M, Kiesewetter DO, et al. (2012) Long-term multimodal imaging of tumor draining sentinel lymph nodes using mesoporous silica-based nanoprobes. Biomaterials 33: 4370-8.

139. Ma Q, Nakane Y, Mori Y, Hasegawa M, Yoshioka Y, et al. (2012) Multilayered, core/shell nanoprobes based on magnetic ferric oxide particles and quantum dots for multimodality imaging of breast cancer tumors. Biomaterials 33: 8486-94.

140. Wang JH, Wang B, Liu Q, Li Q, Huang H, et al. (2013) Bimodal optical diagnostics of oral cancer based on Rose Bengal conjugated gold nanorod platform. Biomaterials 34: 4274-83.

141. Lee SY, Jang SH, Cho MH, Kim YM, Cho KC, et al. (2009) In situ single cell monitoring by isocyanide-functionalized Ag and Au nanoprobe-based Raman spectroscopy. J Microbiol Biotechnol 19: 904-10.

142. Leduc C, Si S, Gautier J, Soto-Ribeiro M, Wehrle-Haller B, et al. (2013) Highly Specific Gold Nanoprobe for Live-Cell Single-Molecule Imaging. Nano Letters 13: 1489-94.

143. Singhal R, Orynbayeva Z, Kalyana Sundaram RV, Niu JJ, Bhattacharyya S, et al. (2011) Multifunctional Carbon-Nanotube Cellular Endoscopes. Nat Nanotechnol 6: 57-64.

144. Yan R, Park JH, Choi Y, Heo CJ, Yang SM, et al. (2012) Nanowire-Based Single-Cell Endoscopy. Nat Nanotechnol 7: 191-6.

145. Actis P, Tokar S, Clausmeyer J, Babakinejad B, Mikhaleva S, et al. (2013) Electrochemical nanoprobes for single-cell analysis. ACS Nano 8: 875-84.

146. Crayton SH, Tsourkas A (2011) pH-Titratable Superparamagnetic Iron Oxide for Improved Nanoparticle Accumulation in Acidic Tumor Microenvironments. ACS Nano 5: 9592-601.

147. Lee H, Akers W, Bhushan K, Bloch S, Sudlow G, et al. (2011) Tang R, Achilefu, S, Near-Infrared pH-Activatable Fluorescent Probes for Imaging Primary and Metastatic Breast Tumors. Bioconjug Chem 22: 777-84.

148. Wong C, Stylianopoulos T, Cui J, Martin J, Chauhan VP, et al. (2011) Multistage nanoparticle delivery system for deep penetration into tumor tissue. Proc Natl Acad Sci 108: 2426-431.

149. Davies A, Lewis DJ, Watson SP, Thomas SG, Pikramenou Z, et al. (2012) pH-controlled delivery of luminescent europium coated nanoparticles into platelets. Proc Natl Acad Sci 109: 1862-7.

150. Mikhaylov G, Mikac U, Magaeva AA, Itin VI, Naiden EP, et al. (2011) Ferri-liposomes as an MRI-visible drug-delivery system for targeting tumours and their microenvironment. Nat Nanotechnol 6: 594-602.

151. Saatchi K, Soema P, Gelder N, Misri R, McPhee K, et al. (2012) Hyperbranched Polyglycerols as Trimodal Imaging Agents: Design, Biocompatibility, and Tumor Uptake. Bioconjug Chem 23: 372-81.

152. Locke LW, Mayo MW, Yoo AD, Williams MB, Berr SS (2012) PET imaging of tumor associated macrophages using mannose coated 64Cu liposomes. Biomaterials 33: 7785-93.

153. Tanabe K, Zhang Z, Ito T, Hatta H, Nishimoto S (2007) Current molecular design of intelligent drugs and imaging probes targeting tumor-specific microenvironments. Org Biomol Chem 5: 3745-57.

154. Iessi EMM, Lozupone F, Fais S, Milito AD (2008) Tumor acidity and malignancy: novel aspects in the design of anti-tumor therapy. Cancer Ther 6: 55-66.

155. Chauhan VP, Popović Z, Chen O, Cui J, Fukumura D, et al. (2011) Fluorescent Nanorods and Nanospheres for Real-Time In Vivo Probing of Nanoparticle Shape-Dependent Tumor Penetration. Angew Chem Int Ed Engl 50: 11417-20.

156. Wang L, Li C (2011) pH responsive fluorescence nanoprobe imaging of tumors by sensing the acidic microenvironment. J Mat Chem 21: 15862-71.

157. Medintz IL, Stewart MH, Trammell SA, Susumu K, Delehanty JB, et al. (2010) Quantum-dot/dopamine bioconjugates function as redox coupled assemblies for in vitro and intracellular pH sensing. Nat Mater 9: 676-84.

158. Jin T, Sasaki A, Kinjo M, Miyazaki J (2010) A quantum dot-based ratiometric pH sensor. Chem Commun 46: 2408-10.

159. Somers RC, Lanning RM, Snee PT, Greytak AB, Jain RK, et al. (2012) A nanocrystal-based ratiometric pH sensor for natural pH ranges. Chem Sci 3: 2980-5.

160. Paek K, Chung S, Cho CH, Kim BJ (2011) Fluorescent and pH-responsive diblock copolymer-coated core-shell CdSe/ZnS particles for a color-displaying, ratiometric pH sensor. Chem Commun 47: 10272-4.

161. Dennis AM, Rhee WJ, Sotto D, Dublin SN, Bao G (2012) Quantum Dot–Fluorescent Protein FRET Probes for Sensing Intracellular pH. ACS Nano 6: 2917-24.

162. Huang G, Si Z, Yang S, Li C, Xing D (2012) Dextran based pH-sensitive near-infrared nanoprobe for in vivo differential-absorption dual-wavelength photoacoustic imaging of tumors. J Mater Chem 22: 22575-81.

163. Qi L, Shao W, Shi D (2013) JAM-2 siRNA intracellular delivery and real-time imaging by proton-sponge coated quantum dots. J Mater Chem B 1: 654-60.

164. Qi L, Gao X (2008) Quantum dot-amphipol nanocomplex for intracellular delivery and real-time imaging of siRNA. ACS Nano 2: 1403-10.

165. Li C, Xia J, Wei X, Yan H, Si Z, et al. (2010) pH-Activated Near-Infrared Fluorescence Nanoprobe Imaging Tumors by Sensing the Acidic Microenvironment. Advan Functi Mater 20: 2222-30.

166. Zhou K, Wang Y, Huang X, Luby-Phelps K, Sumer BD, et al. (2011) Tunable, Ultrasensitive pH-Responsive Nanoparticles Targeting Specific Endocytic Organelles in Living Cells. Angew Chem Int Ed Engl 50: 6109-14.

167. Zhou K, Liu H, Zhang S, Huang X, Wang Y, et al. (2012) Multicolored pH-Tunable and Activatable Fluorescence Nanoplatform Responsive to Physiologic pH Stimuli. J Am Chem Soc 134: 7803-11.

168. Shi W, Li X, Ma H (2012) A Tunable Ratiometric pH Sensor Based on Carbon Nanodots for the Quantitative Measurement of the Intracellular pH of Whole Cells. Angew Chem Int Ed Engl 51: 6432-5.

169. Wu Y, Zhang W, Li J, Zhang Y (2013) Optical imaging of tumor microenvironment. Am J Nucl Med Mol Imaging 3: 1-15.

170. Leung MK, Chow JC, Chithrani BD, Lee MJ, Oms B, et al. (2011) Irradiation of gold nanoparticles by X-rays: Monte Carlo simulation of dose enhancements and the spatial properties of the secondary electrons production. Med Phys 38: 624-31.

171. Anshup A, Venkataraman JS, Subramaniam C, Kumar RR, Priya S, et al. (2005) Growth of gold nanoparticles in human cells. Langmuir 21: 11562-7.

172. Hainfeld JF, Dilmanian FA, Slatkin DN, Smilowitz HM (2008) Radiotherapy enhancement with gold nanoparticles. J Pharm Pharmacol 60: 977-85.

173. Kirui DK, Kalidov I, Wang Y, Batt CA (2013) Targeted near-IR hybrid magnetic nanoparticles for in vivo cancer therapy and imaging. Nanomedicine 9: 702-11.

174. Zhao Y, Sultan D, Detering L, Cho S, Sun G, et al. (2014) Copper-64-alloyed gold nanoparticles for cancer imaging: improved radiolabel stability and diagnostic accuracy. Angew Chem Int Ed Engl 53: 156-9.

175. Amendola V, Scaramuzza S, Litti L, Meneghetti M, Zuccolotto G, et al. (2014) Magneto-plasmonic Au-Fe alloy nanoparticles designed for multimodal SERS-MRI-CT imaging. Small 10: 2476-86.

176. Tang W, Zhen Z, Yang C, Wang L, Cowger T, et al. (2014) Fe5C2 nanoparticles with high MRI contrast enhancement for tumor imaging. Small 10: 1245-9.

177. Johnson L, Spence TZ (2010) Michelle, Probes for Nitric Oxide Research In: Molecular Probes Handbook: A Guide to Fluorescent Probes and Labeling Technologies (11th Edn) Life Technologies Corporation, USA.

178. Alderton WK, Cooper CE, Knowles RG (2001) Nitric oxide synthases: structure, function and inhibition. Biochem J 357: 593-615.

179. Rivera Gil P, Vazquez-Vazquez C, Giannini V, Callao MP, Parak WJ, et al. (2013) Plasmonic Nanoprobes for Real-Time Optical Monitoring of Nitric Oxide inside Living Cells. Angew Chem Int Ed Engl 52: 13694-8.

180. Tian J, Chen H, Zhuo L, Xie Y, Li N, et al. (2011) A highly selective, cell-permeable fluorescent nanoprobe for ratiometric detection and imaging of peroxynitrite in living cells. Chemistry 17: 6626-34.

181. Ferrara N, Gerber HP, LeCouter J (2003) The biology of VEGF and its receptors. Nat Med 9: 669-76.

182. Ferrara N, Kerbel RS (2005) Angiogenesis as a therapeutic target. Nature 438: 967-74.

183. Folkman J (1990) What Is the Evidence That Tumors Are Angiogenesis Dependent? J Natl Cancer Inst 82: 4-6.

184. Stetler-Stevenson WG (2001) The role of matrix metalloproteinases in tumor invasion, metastasis, and angiogenesis. Surg Oncol Clin N Am 10: 383-92.

185. Karathanasis E, Chan L, Karumbaiah L, McNeeley K, D'Orsi CJ, et al. (2009) Tumor Vascular Permeability to a Nanoprobe Correlates to Tumor-Specific Expression Levels of Angiogenic Markers. PLoS ONE 4: e5843.

186. Kim B, Yang J, Hwang M, Choi J, Kim HO, et al. (2013) Aptamer-modified magnetic nanoprobe for molecular MR imaging of VEGFR2 on angiogenic vasculature. Nanoscale Res Lett 8: 399.

187. Kessinger CW, Khemtong C, Togao O, Takahashi M, Sumer BD, et al. (2010) In vivo angiogenesis imaging of solid tumors by αvβ3-targeted, dual-modality micellar nanoprobes. Experi Biol Med 235: 957-65.

188. Aillon KL, Xie Y, El-Gendy N, Berkland CJ, Forrest ML (2009) Effects of nanomaterial physicochemical properties on in vivo toxicity. Adv Drug Deliv Rev 61: 457-66.

189. Hardman RA (2006) Toxicologic Review of Quantum Dots: Toxicity Depends on Physicochemical and Environmental Factors. Environ Health Perspect 114: 165-72.

190. Nel A, Xia T, Mädler L, Li N (2006) Toxic Potential of Materials at the Nanolevel. Science 311: 622-7.

191. Nguyen QT, Olson ES, Aguilera TA, Jiang T, Scadeng M, et al. (2010) Surgery with molecular fluorescence imaging using activatable cell-penetrating peptides decreases residual cancer and improves survival. Proc Natl Acad Sci 107: 4317-22.

192. Olson ES, Jiang T, Aguilera TA, Nguyen QT, Ellies LG, et al. (2010) Activatable cell penetrating peptides linked to nanoparticles as dual probes for in vivo fluorescence and MR imaging of proteases. Proc Natl Acad Sci 107: 4311-6.